

1 **The role of anthropogenic aerosols in the anomalous cooling**
2 **from 1960 to 1990 in the CMIP6 Earth System Models**

3 Jie Zhang¹, Kalli Furtado^{2*}, Steven T. Turnock², Jane P. Mulcahy², Laura J. Wilcox³,
4 Ben B. Booth², David Sexton², Tongwen Wu¹, Fang Zhang¹, Qianxia Liu¹

5 ¹Beijing Climate Center, China Meteorological Administration, Beijing, China, 100081

6 ²Met Office Hadley Centre, Exeter, UK, EX1 3PB

7 ³National Centre for Atmospheric Science, Department of Meteorology, University of Reading, Reading,
8 UK

9 *Corresponding to:* Kalli Furtado (kalli.furtado@metoffice.gov.uk)

10

11 **Abstract** The Earth System Models (ESMs) that participated in the 6th Coupled Model
12 Intercomparison Project (CMIP6) tend to simulate excessive cooling in surface air
13 temperature (TAS) between 1960 and 1990. The anomalous cooling is pronounced over
14 the Northern Hemisphere (NH) midlatitudes, coinciding with the rapid growth of
15 anthropogenic sulfur dioxide (SO₂) emissions, the primary precursor of atmospheric
16 sulphate aerosols. Structural uncertainties between ESMs have a larger impact on the
17 anomalous cooling than internal variability. Historical simulations with and without
18 anthropogenic aerosol emissions indicate that the anomalous cooling in the ESMs is
19 attributed to the higher aerosol burden in these models. The aerosol-forcing sensitivity,
20 estimated as the outgoing shortwave radiation (OSR) response to aerosol concentration
21 changes, cannot well explain the diversity of PHC biases in the ESMs. The relative
22 contributions to aerosol-forcing-sensitivity from aerosol-radiation interactions (ARI)
23 and aerosol-cloud interactions (ACI) can be estimated from CMIP6 simulations. We
24 show that even when the aerosol-forcing-sensitivity is similar between ESMs, the
25 relative contributions of ARI and ACI may be substantially different. The ACI accounts
26 for between 64 to 87% of the aerosol-forcing-sensitivity in the models, and is the main
27 source of the aerosol-forcing sensitivity differences between the ESMs. The ACI can
28 be further decomposed into a cloud-amount term (which depends linearly on cloud
29 fraction) and a cloud-albedo term (which is independent of cloud fraction, to the first
30 order) with the cloud-amount term accounting for most of the inter-model differences.

31

32 1. Introduction

33 Surface air temperature (TAS) variation is an essential indicator of climate change,
34 and reproducing the evolution of historical TAS is a crucial criterion for model
35 evaluation. However, the historical TAS anomaly simulated by the models in the 6th
36 Coupled Model Intercomparison Project (CMIP6) is on average colder than that
37 observed in the mid-twentieth century, whereas the CMIP5 models tracked the
38 instrumental TAS variation quite well (Flynn and Mauritsen, 2020). This is surprising
39 because the transient climate response in CMIP6 models is generally higher than in
40 CMIP5 models (e.g., Flynn and Mauritsen, 2020; Meehl et al., 2020).

41 As a result of anthropogenic emissions, atmospheric aerosol concentrations
42 increased along with rising greenhouse gases, but with greater decadal variability.
43 Aerosols are generally not evenly distributed around the planet as greenhouse gases,
44 and they have relatively short lifetimes of the order of a week. Aerosols increased
45 rapidly in the mid-twentieth century, predominantly due to US and European emissions.
46 The rate of change of global aerosol emissions slowed down in the late 20th century
47 (Hoesly et al., 2018), and the trend of global emission has been negative since the mid-
48 2000s (Klimont et al., 2013). There has also been a shift in emission source regions.
49 European and US emissions have declined following the introduction of clean air
50 legislation since the 1980s, while Asian emissions have risen due to economic
51 development. East Asian emissions clearly increased from 2000 to 2005, followed by
52 a decrease with large uncertainties (Aas et al., 2020). The decade long emission
53 reduction since 2006 over East China is not well represented by the CMIP6 emission
54 (Wang et al., 2021).

55 Although greenhouse warming was concluded to be the dominant forcing for long-
56 term changes (e.g., Weart, 2008; Bindoff et al., 2013), multidecadal variability in TAS
57 and the reduced rate of warming in the mid-twentieth century in particular, has been
58 attributed to aerosol forcing (e.g., Wilcox et al., 2013). Ramanathan and Feng (2009)
59 noted that the aerosol cooling effect might have masked as much as 47% of the global

60 warming by greenhouse gases in the year 2005, with an uncertainty range of 20~80%.
61 The aerosol cooling effect is mainly attributed to the ability of sulphate particles to
62 reflect incoming solar radiation and modify the microphysical properties of clouds (e.g.,
63 Charlson et al., 1990; Mitchell et al., 1995; Lohmann and Feichter, 2005). The increase
64 in anthropogenic aerosols was also responsible for weakening the hydrological cycle
65 between the 1950s and the 1980s (Wu et al., 2013).

66 Previous work has suggested that the anomalous mid-twentieth century cooling in
67 the CMIP6 models is the result of excessive aerosol forcing. Flynn and Mauritsen
68 (2020) suggested that aerosol cooling is too strong in many CMIP6 models because
69 there is no apparent relationship between the warming trends simulated by models and
70 their transient climate responses (TCRs) before the 1970s. ~~The warming trend is larger
71 than observed post 1970 in CMIP6 models, offsetting the pre 1970s cooling.~~ Dittus et
72 al. (2020) found that historical simulations can better capture the observed historical
73 record by reducing the aerosol emissions in HadGEM3-GC3.1, demonstrating an overly
74 strong aerosol cooling effect. ~~They showed that simulations with large anthropogenic
75 aerosol emissions had greater cooling trends between 1951 and 1980, which were
76 significantly different to the observed trend, while simulations with smaller aerosol
77 forcing were more consistent with observations.~~ In this study we characterize the mid-
78 twentieth century excessive cooling in CMIP6 ESMs. In order to quantify the role of
79 aerosol processes in this anomalous cooling, historical experiments with and without
80 anthropogenic aerosol emissions are employed. The remainder of the paper is organized
81 as follows. Section 2 introduces the models, data, and a quantitative method to separate
82 the aerosol forcing components. The major features of anomalous cooling in CMIP6
83 ESMs are examined in section 3. Section 4 investigates the possible reasons for the
84 anomalous cooling. The relative importance of aerosol-radiation interactions and
85 aerosol-cloud interactions in each ESM is quantified and discussed in section 5.
86 Conclusion is given in Section 6.

87

88 2. Model, data, and method

89 2.1 CMIP6 ESMs

90 CMIP6 includes an unprecedented number of models with representations of
91 aerosol-cloud interactions. Many also have interactive tropospheric chemistry and
92 aerosol schemes. Six such ESMs are employed in this study: BCC-ESM1 (Wu et al.,
93 2020; Zhang et al., 2021), EC-Earth-AerChem ([van Noije et al., 2020](#)), GFDL-ESM4
94 (Dunne et al., 2020), MPI-ESM-1-2-HAM ([NeubauerMauritsen et al., 2019](#)),
95 NorESM2-LM (Seland et al., 2020), and UKESM1-0-LL (Sellar et al., 2019). The
96 surface air temperature simulated in corresponding models with lower-complexity are
97 also examined: BCC-CSM2-MR (Wu et al., 2019b), EC-Earth3 (Döscher et al., 2021),
98 and MPI-ESM1-2-LR (Mauritsen et al., 2019) with prescribed tropospheric chemistry
99 and aerosol; GFDL-CM4 (Held et al., 2019), NorCPM1 (Bethke et al., 2019), and
100 HadGEM3-GC31-LL (Williams et al., 2017) with prescribed tropospheric chemistry
101 and interactive aerosol scheme. BCC-CSM2-MR, EC-Earth3, and MPI-ESM1-2-LR
102 prescribe the anthropogenic aerosol forcings using the MACv2-SP parameterization
103 (Stevens et al., 2017). MACv2-SP approximates the observationally constrained spatial
104 distributions of the monthly mean anthropogenic aerosol optical properties and an
105 associated Twomey effect. ~~Except for BCC models, the horizontal resolutions of the~~
106 ~~ESMs are the same as the corresponding lower complexity models.~~ A brief summary
107 of the ESMs and the lower-complexity models is introduced in Table 1.

108 **Table 1.** Information of the ESMs with interactive chemistry and aerosol scheme, as
 109 well as the corresponding lower-complexity models.

Modeling group	ESM (Atmospheric Resolution)	Lower-complexity models (Atmospheric Resolution)	Prescribed tropospheric chemistry	Prescribed aerosol	Number of members	References
Beijing Climate Center (BCC)	BCC-ESM1: the BCC Earth System Model version 1 (T42, 26 layers to 2.914 hPa)	BCC-CSM2-MR: the median resolution BCC Climate System Model version 2 (T106, 46 layers to 1.459 hPa)	Y	Y	3	Wu et al.(2019b, 2020); Zhang et al. (2021)
European consortium of meteorological services, research institutes, and high-performance computing centres	EC-Earth-AerChem: the EC-Earth configuration with interactive aerosols and atmospheric chemistry (T255, 91 layers to 0.01 hPa)	EC-Earth3: the EC-Earth version 3 (T255, 91 layers to 0.01 hPa)	Y	Y	1	von Noije et al. (2020); Döscher et al. (2021)
US Department of Commerce/NOAA / Geophysical Fluid Dynamics Laboratory (GFDL)	GFDL-ESM4: the GFDL Earth System Model version 4 (C96, 49 layers to 1 hPa)	GFDL-CM4: the GFDL Climate Model version 4 (C96, 33 layers to 1 hPa)	Y	N	1	Dunne et al. (2020); Held et al. (2019)
Max Planck Institute for Meteorology (MPI)	MPI-ESM-1-2-HAM: the HAMMOZ-Consortium of MPI Earth System Model (T63, 47 layers to 0.01 hPa)	MPI-ESM1-2-LR: the lower-resolution version of MPI Earth System Model (T63, 47 layers to 0.01 hPa)	Y	Y	3	Neubauer et al.(2019); Mauritsen et al. (2019);
Norwegian Climate Center (NCC)	NorESM2-LM: the lower-resolution of Norwegian ESM version 2 (About 2°, 32 layers to 2 hPa)	NorCPM1: the Norwegian Climate Prediction Model version 1 (About 2°, 26 layers to 3 hPa)	Y	N	3	Seland et al. (2020); Bethke et al. (2019)
Met Office's Hadley Centre for Climate Prediction and Research (MOHC)	UKESM1-0-LL: U.K. Earth System Model version 1 (N96, 85 layers to 85 km)	HadGEM3-GC31-LL: the Hadley Centre Global Environment Model in the Global Coupled configuration 3.1 (N96, 85 layers to 85km)	Y	N	3	Sellar et al. (2019); Williams et al. (2017)

111 **2.2 Data**

112

113

Table 2 Variables used in this study.

Variable name	CMIP6 diagnostic label	Description	Units
TAS	tas	Surface air temperature	°C
OSR	rsut	All-sky outgoing shortwave radiation at the top of atmosphere (TOA)	W m ⁻²
OSRclr	rsutcs	OSR assuming clear sky	W m ⁻²
mmrso4	mmrso4	Mass mixing ratio of sulphate aerosol in the atmosphere	kg kg ⁻¹
CLT	clt	Total cloud amount	%
r _{eff}	refffclwtop	cloud-top effective droplet radius	µm
loadSO4		Sulphate loading in the atmosphere, calculated from mmrso4	mg m ⁻²
OSRclr_hist		Mean OSRclr in the historical simulation from 1850 to 1990	W m ⁻²
CLT_hist		Mean CLT in the historical simulation from 1850 to 1990	%

114

115 The CMIP6 historical experiment and hist-piAer experiment are employed. The
 116 historical experiment is forced by time-evolving, externally imposed natural and
 117 anthropogenic forcings, such as solar variability, volcanic aerosols, greenhouse gases,
 118 and aerosol emissions (Eyring et al., 2016). The hist-piAer experiment is designed by
 119 the CMIP6-endorsed Aerosol Chemistry Model Intercomparison Project
 120 (AerChemMIP; Collins et al., 2017). It is run in parallel with the historical experiment
 121 but fixes aerosol and aerosol precursor emissions to pre-industrial conditions.
 122 Therefore, the differences between these two experiments are attributable to
 123 anthropogenic aerosol emissions. The design of the hist-piAer simulation means that it

124 can also capture any nonlinearities resulting from GHG-driven changes in clouds. This
125 is in contrast to the hist-aer simulations available from the Detection and Attribution
126 Model Intercomparison Project (DAMIP; Gillett et al., 2016), which resembles the
127 historical simulations but are only forced by transient changes in aerosol.

128 The monthly outputs from historical and hist-piAer simulations for ESMs are used,
129 including TAS, all-sky outgoing shortwave radiation at the top-of-atmosphere (OSR),
130 OSR assuming clear sky (OSRclr), mass mixing ratio of sulphate aerosol in the
131 atmosphere (mmrso4), total cloud amount (CLT), and cloud-top effective droplet radius
132 (r_{eff}). These variables are summarized in Table 2. The corresponding lower-complexity
133 models have conducted the historical but not the hist-piAer simulations, and only the
134 monthly TAS output from the historical simulations are used. Therefore, we focus on
135 the ESMs when identifying the main aerosol processes contributing to the anomalous
136 cooling.

137 The verification data used in this study is HadCRUT5, the monthly 5°lat by 5°lon
138 gridded surface temperature (Morice et al., 2021), a blend of the Met Office Hadley
139 Centre SST data set HadSST4 (Kennedy et al., 2019) and the land surface air
140 temperature CRUTEM5 (Osborn et al., 2021).

142 2.3 Method

143 By comparing the TAS anomalies in ESMs and the lower-complexity models with
144 HadCRUT5, our study found that TAS anomalies from 1960 to 1990 relative to 1850-
145 1900 in ESMs and most of the lower-complexity models are on average much lower
146 than observed, resembling a "pot-hole" shape. The magnitude of this is period of
147 anomalous cooling, i.e., the "pot-hole" cooling (PHC), is ~~then~~ quantified as the near-
148 global mean (60°S to 65°N) difference in the TAS anomaly between models and
149 HadCRUT5 from 1960 to 1990. The variations over the polar regions (north of 65°N
150 and south of 60°S) are not considered due to the lack of long-term reliable observations
151 (Wu et al., 2019a). ~~The PHC period coincides with a period when global emissions of~~

152 ~~SO₂, the main precursor of sulphate aerosol, rapidly increased.~~

153 The aerosol cooling ~~due to aerosol-radiation interaction (ARI)~~ is dominated by the
154 contribution of sulphate aerosol as estimated by models and observations (Myhre et al.,
155 2013; [Smith et al., 2020](#)). We use the evolution of sulphate loading (loadSO4) through
156 the historic simulation as a proxy for total aerosol concentration changes to link
157 estimates of the impact of ~~aerosol-forcing-sensitivity~~aerosol forcing. Whilst the overall
158 impact of aerosol forcing will also ~~be driven by~~depend on other aerosol species, we
159 adopt this approach because the sulphates dominate estimates of ~~aerosol-forcing-~~
160 ~~sensitivity~~aerosol forcing during this period and other aerosols species can be assumed
161 (as a 1st order approximation) to have covaried with the SO₂ emissions during this
162 period as presented by the Community Emissions Data System (CEDS) inventory
163 adopted by CMIP6 models (Hoesly et al, 2018). As such when we present estimates of
164 the aerosol impact/loadSO4 we are presenting the impact of all aerosol species
165 (including absorbing aerosols such as black carbon) as they covary with the sulphate
166 concentrations during the historic period. The motivation for presenting it in this way,
167 is we can separate differences in ESM responses to changes in aerosol amount from the
168 differences in aerosol amount (represented by loadSO4) simulated by the ESMs.

169 We can estimate the impact of anthropogenic aerosol by using the difference in
170 OSR between the historical and hist-piAer simulations, ΔOSR . ΔOSR ~~is~~ of course
171 involves any differences in natural variability and planetary albedo, between the two
172 simulations, including clear-sky albedo changes and any adjustments in the
173 microphysical or macroscopic properties of clouds. The sensitivity of the OSR-
174 response to aerosol changes, i.e., the aerosol-forcing-sensitivity, can be measured by
175 the linear fit slope between the annual mean globally averaged OSR differences and
176 loadSO4 differences between the historical and hist-piAer simulations:

$$177 \quad \underline{\text{Aerosol-forcing-sensitivity}} = \Delta OSR / \Delta \text{loadSO4}. \quad (1)$$

178 ~~Wileox et al. (2015) found a large diversity of the CMIP5 models in simulating~~
179 ~~the total aerosol forcing, which arises from the diversity in global load and spatial~~
180 ~~distribution of sulphate aerosol, and differences in global mean cloud top effective~~

181 ~~radius, amongst other factors.~~

182 In this study, we diagnose the OSR differences from historical simulations that
183 also capture the temperature response. As such the OSR differences do not represent a
184 measure of only the aerosol forcing impact but combine OSR differences arising from
185 both the aerosol forcing and the temperature response to this forcing, which we refer to
186 in this manuscript as the aerosol-forcing-sensitivity. It presents a measure of the
187 importance of aerosol changes in simulated temperature changes that can be easily
188 calculated for existing transient simulations. The aerosol-forcing-sensitivity is different
189 from the commonly used aerosol effective radiative forcing (ERFaer), which is the
190 change in net TOA downward radiative flux after allowing adjustments in the
191 atmosphere, but with sea surface temperatures and sea ice cover are fixed at
192 climatological values. The ERFaer for each ESM except MPI-ESM-1-2-HAM is listed
193 in Table 3 and compared with the aerosol-forcing-sensitivity in section 4.

194 The aerosol-forcing-sensitivity can be further partitioned into a contribution from
195 aerosol-radiation interactions (ARI), and aerosol-cloud interactions (ACI). ARI and
196 ACI can be readily estimated from the CMIP6 output because annual mean cloud
197 amount (CLT), OSR, and the OSR *assuming only clear-sky* (OSRclr), are available for
198 all the CMIP6 ESMs. For each model, the clear-sky part OSR, OSRclr_p, can be
199 estimated as (1-CLT/100.)*OSRclr. The aerosol-forcing-sensitivity in clear-sky part
200 can therefore be estimated as:

$$\begin{aligned} \Delta OSRclr_p / \Delta loadSO4 = & (1-CLT_{hist}/100.) * \Delta OSRclr / \Delta loadSO4 \\ & - OSRclr_{hist} / 100 * \Delta CLT / \Delta loadSO4 + residual_{clr}, \quad (2) \end{aligned}$$

203 where CLT_hist and OSRclr_hist are the mean CLT and OSRclr in the historical
204 experiment. The aerosol-forcing-sensitivity in cloudy part are relative to cloud amount
205 response to aerosol loading and cloud radiative effect changes and can be estimated as:

$$\begin{aligned} \Delta OSRcld_p / \Delta loadSO4 = & A * \Delta CLT / \Delta loadSO4 + cloud-albedo term \\ & + residual_{cld}. \quad (3) \end{aligned}$$

208 Therefore, the aerosol-forcing-sensitivity can be decomposed as:

$$\begin{aligned}
209 \quad \underbrace{\Delta OSR / \Delta loadSO4}_{\text{Aerosol-forcing-sensitivity}} &= (1-CLT_{hist}/100) * \Delta OSR_{clr} / \Delta loadSO4 \\
210 &+ (A-OSR_{clr}_{hist}/100.) * \Delta CLT / \Delta loadSO4 \\
211 &+ \text{cloud-albedo term} + \text{residual} \\
212 &= \underbrace{(1-CLT_{hist}/100) * M}_{\text{Aerosol-rad. Interactions (ARI)}} + \underbrace{(A-OSR_{clr}_{hist}/100.) * N}_{\text{cloud-amount term}} \\
213 &+ \text{cloud-albedo term} + \text{residual}, \quad (4) \\
214 &
\end{aligned}$$

215 where M, N and A are empirically determined parameters. The parameter M is the
216 slope of a linear fit of ΔOSR_{clr} to $\Delta loadSO4$, and therefore measures the strength of
217 the aerosol-radiation interactions in each model. The first term on the right-hand side
218 of Eq. (4), $(1-CLT_{hist}/100.) * M$, can therefore be identified with ARI. The parameter
219 A is the slope of a linear fit of ΔOSR_{clr} to ΔCLT , and therefore measures the
220 correlation of the shortwave radiation reflected by clouds with changes in cloud
221 amount. That is, the parameter A represents the baseline cloud albedo which is sensitive
222 to the cloud parameterizations via Cloud Droplet Number Concentration (CDNC),
223 cloud-droplet effective radius, and other factors. The parameter N is the slope of a linear
224 fit of ΔCLT to $\Delta loadSO4$, and therefore measures the sensitivity of cloud amount to
225 aerosols. Note that changes in cloud amount by definition also affect the fraction of
226 clear-sky, hence increases in OSR_{clr} due to increases in CLT (i.e., $A * N$) can be partly
227 offset by changes in area of clear-sky containing aerosols ($OSR_{clr}_{hist}/100. * N$). The
228 second term on the right-hand side of Eq. (4), $(A-OSR_{clr}_{hist}/100.) * N$, can therefore
229 contribute to the ACI. Specifically, it is the part of ACI that is linearly proportional to
230 changes to cloud fraction, which we will refer to in this manuscript as the cloud-amount
231 term. It is ~~roughly analogous to the “cloud lifetime effect” (Albrecht, 1989), but~~
232 ~~is therefore~~ sensitive to *any* aerosol-induced cloud fraction changes (Lohmann and
233 Feichter, 2005), including any slow adjustments in clouds due to feedbacks within the
234 Earth System.

235 In addition to depending on ΔCLT , ACI is also influenced by any changes in
236 cloud-albedo that might occur independently of cloud-amount changes. Such

237 adjustments would include increases in cloud droplet number concentration and
238 increases in simulated cloud-droplet effective radius without accompanying changes in
239 cloud cover. Changes purely in the brightness of clouds, without changes in
240 macroscopic properties of clouds, are difficult to identify from the CMIP6 output
241 because all the bulk-properties of clouds co-vary over the course of the projections.
242 However, subtracting ARI and the cloud-amount term from the aerosol-forcing-
243 sensitivity gives a residual that is, by definition, linearly independent of cloud fraction
244 differences (since by construction these have been regressed out). This residual can then
245 be interpreted as due to differences in the albedo of clouds between the historical and
246 hist-piAer, and will be called the "cloud-albedo term". Note that this method of
247 calculation implies that purely albedo effects cannot be distinguished from general
248 residual terms that result from the linear approximation made.

249 Decomposition of the ARI, the cloud-amount term and cloud-albedo term of ACI
250 are detailed further in the Appendix. The aerosol-cloud feedbacks are mainly in the ACI
251 term which includes cloud spatial extent (amount), ~~cloud longevity (lifetime)~~, cloud
252 albedo on radiative fluxes, and cloud particle swelling by humidification (Christensen
253 et al., 2017; Neubauer et al., 2017). There is also a (smaller) effect of feedback on the
254 ARI term that is also affected by cloud amount changes insofar as increased/decreased
255 cloud cover can obscure/reveal clear-sky radiative fluxes. We acknowledge that the
256 linear approximation in our method doesn't explicitly account for the absorption above
257 clouds, or the adjustments to aerosol-radiation interactions (e.g., Carslaw et al., 2013)
258 that are known to be locally important. Our formulation explicitly assumes that there is
259 a broadly linear relationship between loadSO4 and emissions, and aerosol radiation
260 with loadSO4 (and non-linearity due to cloud albedo or amount or any interaction is
261 small at global scale as suggested in Booth et al. (2018)). Should these interaction terms
262 be non-negligible in this analysis, we still expect the broader attribution of the reasons
263 for the model diversity in temperature response over the PHC period, either how they
264 simulate aerosol concentrations or how they simulate the response to this, to generally
265 hold.

This decomposition method is an approximate approach designed to be used with existing simulations, rather than a strict decomposition by dedicated simulations/output variables not included in CMIP6. It can't tell us precise information about each interaction and adjustment, but it can give us an indication of why models behave differently.

Note that our decomposed ACI does not correspond exactly to the definitions of "first" and "second" aerosol indirect effects. For example, the first indirect effect is properly defined as variations of aerosol forcing when cloud droplet number concentration varies at a constant value of the cloud liquid water path. This effect cannot be isolated from the available CMIP6 output.

3. The "pot-hole" bias in CMIP6 ESMs

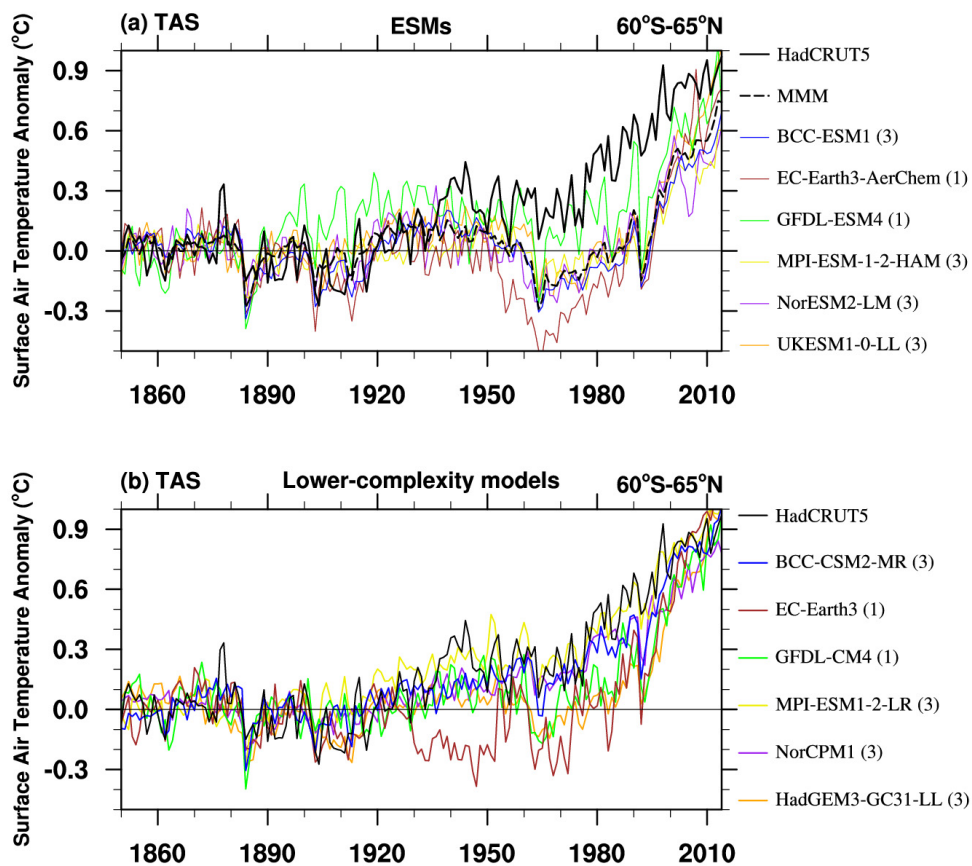


Figure 1. (a) Historical near-global mean (60°S to 65°N) surface air temperature (TAS) anomalies relative to 1850-1900 mean from HadCRUT5 (thick black line), the multi-member ensemble mean for each ESM (MMM, solid color lines), and multi-model mean their ensemble (MMEMMM,

284 dashed black line). (b) is the same as (a), but for the lower-complexity models. ~~The baseline is from~~
285 ~~1850 to 1900.~~ Units: °C. Value in bracket is the number of available members for each model.

286
287 Figure 1a shows the near-global averaged time series of annual mean TAS
288 anomaly relative to 1850 to 1900 in HadCRUT5 during the historical period from 1850
289 to 2014, and the ensemble means for each model except for EC-Earth3-AerChem and
290 GFDL-ESM4 (where only a single realization is available for the hist-piAer
291 experiment). The unforced, long-term drifts in TAS may occur in some of the ESMs,
292 as estimated by their control simulation under pre-industrial conditions (Yool et al.,
293 2020). We have not accounted for long-term control simulation drifts in our study as
294 we are assuming that our focus on inter-decadal scale variability of TAS anomalies is
295 likely to be fairly insensitive to any century scale drifts.

296 The TAS anomaly in HadCRUT5 is generally above the baseline climate from the
297 1940s onwards, and warms fastest from the 1980s to 1990s. Compared with the
298 observations, all the ESM simulations have negative TAS anomaly biases after the
299 1940s, which are also evident in the ensemble-mean historical TAS of 25 CMIP6
300 models with and without interactive chemistry schemes (Flynn and Mauritsen, 2020).
301 In the ESMs and their ensemble mean (MMM), the cold anomaly biases resemble a
302 "pot-hole" shape (Fig. 1a), which is relatively small before the 1950s and after the 2000s
303 but prominent expands from the 1960s to 1990s. To reduce the impact of the change in
304 the spatial pattern of the emissions in the late 20th century, and the Pinatubo eruption
305 in the early 1990s, we mainly focus on the excessively cold anomaly from 1960 to 1990
306 in this study. The impacts from the Agung (1963) and El Chichon (1982) eruptions have
307 been left in the PHC period as their effect on the simulated temperature is not as
308 pronounced as the response to Pinatubo and are short-lived in time compared to the
309 period we study. The period of anomalous cold in the global mean from 1960 to 1990
310 in model simulations is defined as the "pot-hole" cooling (PHC). Table 3 shows the
311 TAS anomaly biases in two ~~typical~~ periods, the pre-PHC period (1929~1959) and the
312 PHC period (1960~1990). The cold bias in the MMM is -0.14 in the pre-PHC period

313 and intensified to -0.40 in the PHC period. The PHC bias ranges from -0.20°C to -
 314 0.58°C among the ESMs with a standard deviation of 0.11°C. Intra-model spread of
 315 PHC is relatively smaller. That is, model structural uncertainty is more responsible for
 316 PHC than internal climate variability.

317

318 **Table 3.** Biases in near-global averaged TAS anomalies relative to 1850-1900 from the
 319 ensemble mean and standard deviation (SD) for each ESM and the corresponding
 320 lower-complexity model in the pre-PHC (1929~1959) and the PHC period. Biases are
 321 relative to the HadCRUT5. The MMM and the SD of the ESMs are shown in the bottom
 322 row. The aerosol effective forcing (ERFaer) is also shown for each ESM. Note that the
 323 relevant fixed-SST simulations to calculate ERF were not available for MPI-ESM-1-2-
 324 HAM.

ESMs	<u>pre-PHC</u>	PHC	<u>ERFaer</u>	Lower-complexity models	<u>pre-PHC</u>	PHC
	<u>Ensemble mean</u> (SD)	<u>Ensemble mean</u> (SD)			<u>Ensemble mean</u> (SD)	<u>Ensemble mean</u> (SD)
BCC-ESM1	-0.12 (0.01)	-0.45 (0.07)	<u>-1.47</u>	BCC-CSM2-MR	-0.09 (0.01)	-0.10 (0.01)
EC-Earth-AerChem	-0.27	-0.58	<u>-1.1</u>	EC-Earth3	-0.37	-0.37
GFDL-ESM4	-0.02	-0.20	<u>-0.70</u>	GFDL-CM4	-0.12	-0.26
MPI-ESM1-2-HAM	-0.16 (0.01)	-0.39 (0.03)	<u>—</u>	MPI-ESM1-2-LR	0.03 (0.03)	0.01 (0.01)
NorESM2-LM	-0.16 (0.04)	-0.41 (0.04)	<u>-1.21</u>	NorCPM1	-0.10 (0.03)	-0.08 (0.04)
UKESM1-0-LL	-0.10 (0.09)	-0.38 (0.08)	<u>-1.1</u>	HadGEM3-GC31-LL	-0.16 (0.02)	-0.33 (0.03)
MMM	-0.14 (0.08)	-0.40 (0.11)				

325

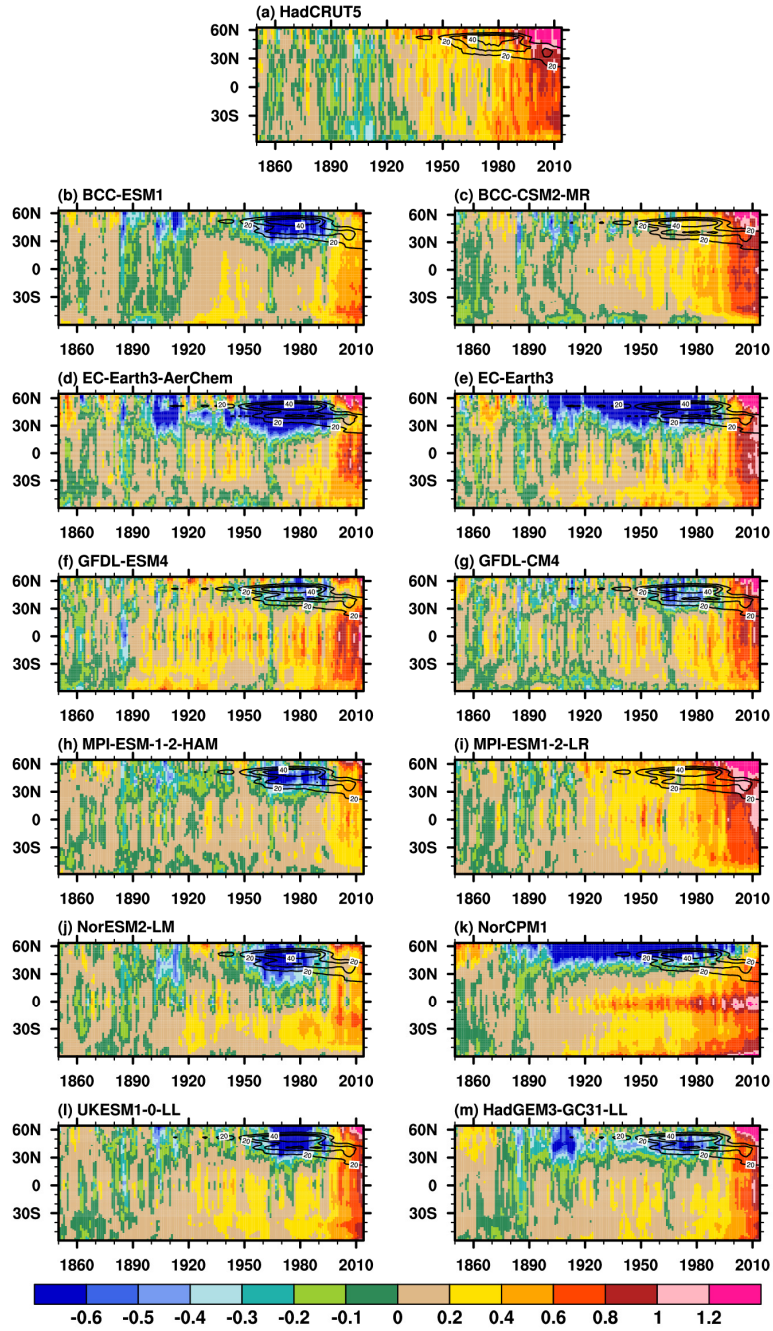
326 The PHC bias is generally smaller in the corresponding lower-complexity models

327 (Fig.1b and Table 3). For models with prescribed chemistry and aerosol (BCC-CSM2-
328 MR and MPI-ESM1-2-LR), the TAS anomaly are reasonably reproduced during the
329 pre-PHC period and the PHC period. The PHC bias are large (-0.37°C) in EC-Earth3,
330 which has prescribed chemistry and aerosol. The large bias may be a reflection of the
331 large internal variability on TAS in EC-Earth3 (Döscher et al., 2021), for which we
332 have only one member. For models with prescribed chemistry and interactive aerosol
333 scheme (GFDL-CM4 and HadGEM3-GC31-LL), the cold biases during the PHC
334 period are comparable with that in the corresponding ESMs. ~~NorCPM1 is due to the~~
335 ~~overestimated tropical and southern hemispheric warming (Fig.2k).~~

336 The spatial and temporal evolution of evolution-of zonal-mean annually averaged
337 TAS anomalies in HadCRUT5, and the MMM for each ESM and lower-complexity
338 model are further examined (in Fig.2). In HadCRUT5, TAS anomalies are generally
339 positive after the 1940s. The most significant TAS anomalies are evident in the late 20th
340 Century and at the beginning of the 21st Century, especially over the NH midlatitudes.
341 The results from BCC-CSM2-MR and MPI-ESM1-2-LR agree well with the
342 observations. However, the ESMs and the other lower-complexity models simulate
343 pronounced cold anomalies over NH subtropical-to-high latitudes during the PHC
344 period. The overestimated tropical and southern hemispheric warming in NorCPM1
345 offsets most of the cooling biases over NH subtropical-to-high latitudes.

346 Surface anthropogenic SO₂ emissions rapidly increase during the PHC period (the
347 line contours in Fig.2). The latitudes of the cooling centers in the ESMs and lower-
348 complexity models with interactive aerosol scheme are spatially co-located with the
349 SO₂ emission sources – North America and East Asia (at around 30°N) and Western
350 Europe (at around 50°N). Generally, the different behaviours seen in Fig.1 and Fig.2
351 suggest that aerosol forcings may be overestimated in the ESMs and lower-complexity
352 models with interactive aerosol scheme, and the anomalous cooling is a result of the
353 extra complexity associated with aerosol processes.

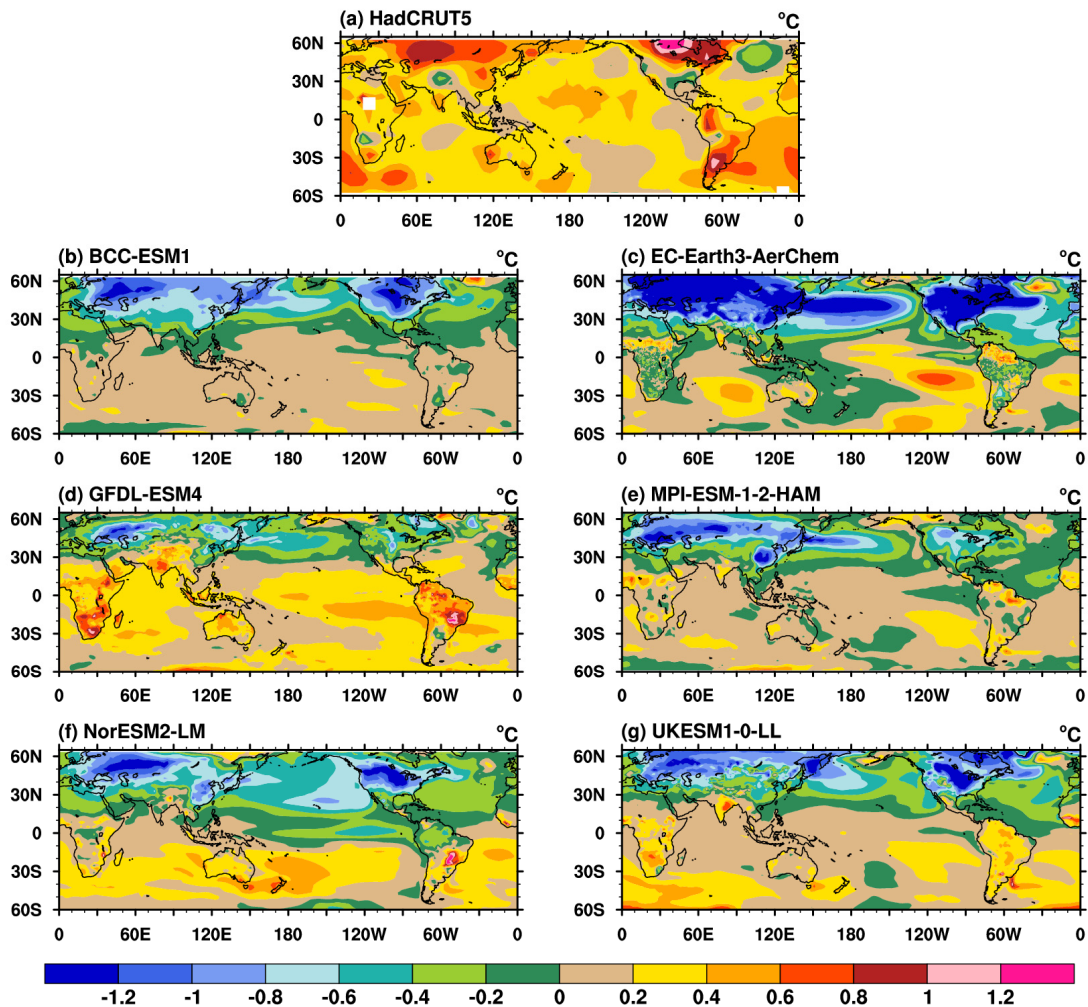
354



355

356 **Figure 2.** Time-latitude cross-section for annual-mean TAS anomalies (shaded) from (a) HadCRUT5,
 357 the ensemble mean MMM for each ESM (left panel), and the corresponding lower-complexity model
 358 (right panel). The anomalies are related to the 1850 ~ 1900 mean. Units: °C. Note that the color scale
 359 intervals in the positive and negative directions are 0.2°C and -0.1°C, respectively. Line contours range
 360 from 20 to 40 ng m⁻² s⁻¹ with an interval of 10 ng m⁻² s⁻¹ show the zonal mean anthropogenic surface SO₂
 361 emission provided by CMIP6.

362



363

364

365 **Figure 3.** The TAS anomalies during the “pot-hole” period (1960 ~ 1990) from (a) HadCRUT5 and (b-
 366 g) the MMMs inensemble mean for each of theESMs. The anomalies are relative to the 1850~1900
 367 mean. Units: °C.

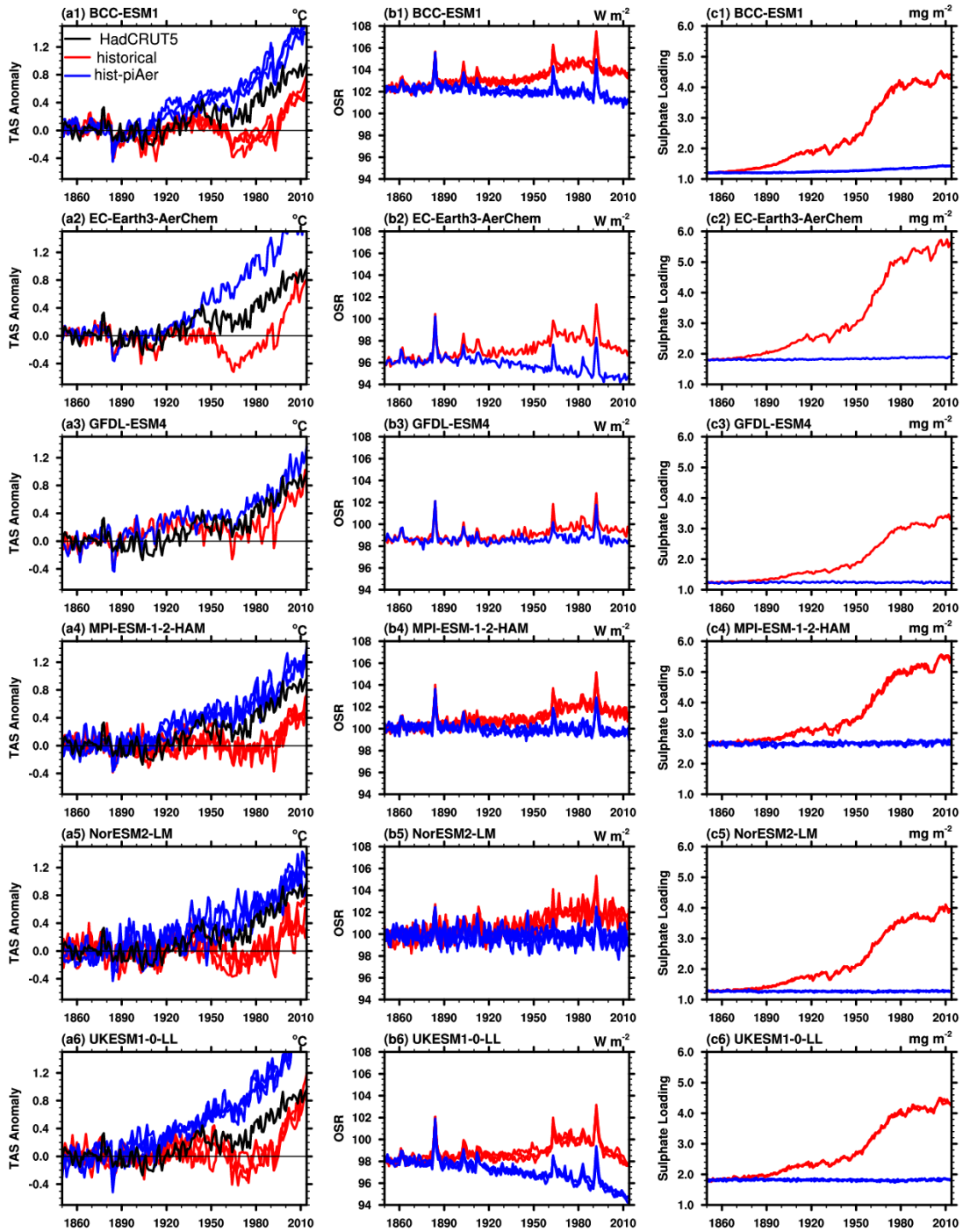
368

369 Figure 3 examines the spatial structure of TAS anomalies in HadCRUT5 and
 370 ESMs inDuring the PHC period. The TAS anomalies in HadCRUT5 are generally
 371 positive and are the largest over Eurasia and North America (Fig.3a). The warm
 372 anomalies are on average more than 0.4 °C along the 30°N ~ 60°N latitudinal belt.
 373 However, the ESMs show anomalies with the opposite sign (Fig.3b-3g) as do the lower-
 374 complexity models with interactive aerosol scheme (figures not shown). The PHC is
 375 pronounced over major SO₂ emission centers (Western Europe, East Asia, and the east
 376 US) and their downstream regions. The cold anomalies over Eurasia and North America

377 are lower than -0.6°C in the ESMs. The PHC biases are strongest at lower levels
 378 (Figures not shown), which is distinct from the amplified upper-tropospheric warming
 379 response to greenhouse gases.

380
 381 **4. Possible reasons for the excessive cooling**

382



383

384

385 **Figure 4.** Evolutions of global annual means of (a1-a6) TAS anomalies (left panel, units: $^{\circ}\text{C}$.), (b1-b6)

386 outgoing shortwave radiation at TOA (OSR, middle panel, units: $W m^{-2}$), and (c1-c6) sulphate loading
387 (right panel, units: $mg m^{-2}$) in HadCRUT5 (black line), each ESM member of the historical (red lines),
388 and hist-piAer experiments (blue lines). The TAS anomalies are relative to the 1850~1900 mean.

389

390 The differences between the historical and hist-piAer simulations help to
391 investigate the impact of anthropogenic aerosol emissions and its possible contribution
392 to the PHC biases. In this section, we examine the TAS, OSR, and sulphate loading
393 differences, and look in detail at their relationship. As shown by the evolution of TAS
394 anomalies in the two experiments (Fig.4, left panel), during the PHC period TAS
395 anomalies in HadCRUT5 (black line) are higher than those in the historical members
396 but lower than those in the hist-piAer members in all ESMs. That is, the model
397 responses to anthropogenic aerosol emissions are larger than the amplitude of the PHC.

398 The temporal evolution of the OSR corresponds with that of the TAS but occurs in the
399 opposite direction (middle panel). ~~The OSR differences between the historical and hist-~~

400 ~~piAer simulations are larger in the ESMs that show big TAS differences (e.g. EC-~~
401 ~~Earth3-AerChem and UKESM1-0-LL).~~ The sulphate loading differences are relatively

402 small in the 19th Century, mildly increase in the first half of the 20th Century, grow most
403 rapidly during the PHC period, and remain high afterward (right panel). The growing

404 sulphate loading during the PHC period corresponds with the increase in northern-
405 hemisphere anthropogenic surface SO₂ emissions (line contours in Fig.2). In

406 comparison with the TAS and OSR differences, the intra-model spread of sulphate
407 loading for each ESM is relatively small. However, the inter-model diversity of

408 sulphate loading is large. For example, the sulphate loading difference between the
409 historical and hist-piAer experiments around the year 2000 is about $4 mg m^{-2}$ in EC-

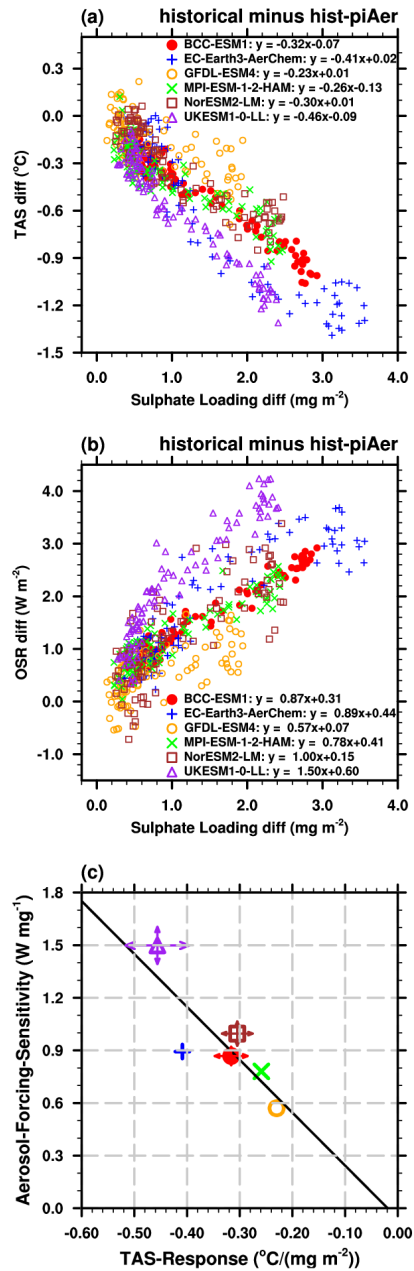
410 Earth3-AerChem, almost twice of that in GFDL-ESM4. With similar anthropogenic
411 SO₂ emission rates, the lower sulphate loading difference in GFDL-ESM4 indicates it

412 has a shorter sulphate aerosol residence time than that in EC-Earth3-AerChem, which
413 may be due to their different sulphate production and deposition schemes. The sulphate

414 loading diversity is also evident in CMIP5 models and is partly responsible for the

415 diversity in modeled radiative forcing (Wilcox et al., 2015).

416 The latitudinal movement of the SO₂ emission center from the 1990s affects the
417 relative strength of aerosol forcing. Due to the more rapid oxidation and higher
418 incoming solar flux at lower latitudes, an equatorward shift in SO₂ emissions around
419 1990s result in a more efficient production of sulphate and stronger aerosol forcing
420 (Manktelow et al., 2007). The northern mid-latitude temperature is also more sensitive
421 to the distribution of aerosols, which is approximately twice as large as the global
422 average (Collins et al., 2013; Shindell and Faluvegi, 2009). Therefore, we focus on the
423 relationships between TAS, OSR and sulphate loading after 1900 when SO₂ emissions
424 changes are dominated by its anthropogenic component, and before 1990. ~~to reduce the~~
425 ~~effects of spatial changes in anthropogenic SO₂ emission centers and the uncertainty of~~
426 ~~model response to the 1991 Mount Pinatubo eruption.~~ As shown in Fig.6a, the TAS
427 differences between the historical and hist-piAer simulations vary approximately
428 linearly with the differences in the sulphate loading. The OSR differences are
429 approximately ~~also~~ linearly correlated with sulphate loading differences (Fig.6b). In
430 both cases, the approximation of linearity holds less well for UKESM1-0-LL,
431 especially at small sulphate loadings. This reflects the behaviour of HadGEM2, a
432 predecessor of UKESM1 (Wilcox et al., 2015), and is likely to be due to the strong
433 aerosol-cloud albedo effect in these models. The global mean annual mean reff
434 decreases by about 0.7 μm since pre-industrial era, more than twice the magnitude of
435 change seen in the other models (Fig.1b in Wilcox et al., 2015 and Fig.9b in this study).



436

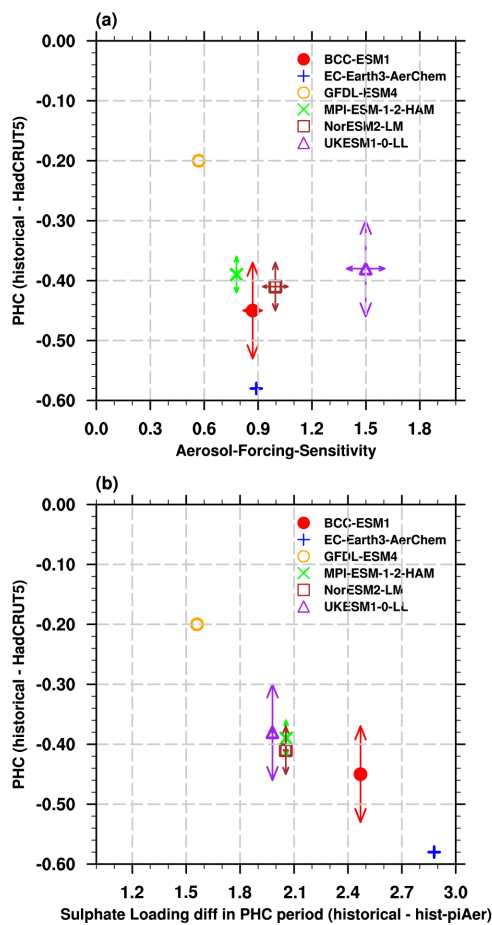
437 **Figure 5.** Scatter plots of 1900-1990 yearly sulphate loading differences between the historical and hist-
 438 piAer simulations (x-axis) versus (a) TAS differences and (b) OSR (y-axis). Results are from [the](#)
 439 [ensemble mean for MMM in](#) each ESM. The captions are the linear fitting equations. (c) shows the TAS
 440 response (x-axis) and aerosol-forcing-sensitivity (y-axis) which is equal to slope of linear fitting for each
 441 ESM (markers), and the corresponding intra-model spread (arrows).

442

443 The slope of the linear fitting equation between TAS (OSR) and sulphate loading
 444 as shown in the captions in Fig. 5a (Fig. 5b) is a measure of the sensitivity of TAS
 445 (aerosol forcing) to perturbations in atmospheric aerosol. Moreover, TAS-response and

446 aerosol-forcing-sensitivity are linearly correlated across the ESMs (Fig.5c). That is, the
 447 strength of the TAS-response can be understood as the magnitude of aerosol-forcing-
 448 sensitivity within each ESM. ~~The similarities between the strength of TAS-response~~
 449 ~~and aerosol forcing sensitivity indicate the dominant role of the aerosol cooling effect.~~
 450 The TAS-response and aerosol-forcing-sensitivity is the lowest in GFDL-ESM4. The
 451 TAS-response and aerosol-forcing-sensitivity in UKESM1-0-LL (the purple marker in
 452 Fig.6c) are the strongest, as well as their intra-model spread (the length of arrows),
 453 indicating that TAS and aerosol forcing in this model are relatively more susceptible to
 454 changes in aerosol. The aerosol-forcing-sensitivity is not correlated with the aerosol
 455 effective radiative forcing (ERFaer, Table 3), largely due to the strong influence of
 456 UKESM1-0-LL on the result.

457



458

459 **Figure 6.** Pot-hole Cooling (PHC) bias in ESMs (°C) versus (a) the aerosol-forcing-sensitivity (W mg⁻¹)

460 and (b) sulphate loading differences (mg m^{-2}) during the PHC period. The arrows show the uncertainty
461 ranges among the members in each ESM.

462

463 Considering the close relationship between TAS anomalies and aerosol loading
464 (Fig.5a), and the impact of aerosol-forcing-sensitivity on the TAS response in ESMs
465 (Fig.5c), their relative contributions to the PHC biases are examined. Figure 6a shows
466 the PHC biases versus the aerosol-forcing-sensitivity (markers) and their intra-model
467 spread (arrows). GFDL-ESM4 has the weakest aerosol-forcing-sensitivity ($\sim 0.60 \text{ W}$
468 mg^{-1}) and the smallest PHC ($-0.20 \text{ }^\circ\text{C}$). However, the relationship between the PHC
469 biases and the aerosol-forcing-sensitivity among the ESMs is not clear: ESMs have
470 similar PHC biases (MPI-ESM, NorESM2, and UKESM1) show large differences in
471 the aerosol-forcing-sensitivity, ranging from 0.78 to 1.5 W mg^{-1} ; the aerosol-forcing-
472 sensitivity in EC-Earth3-AerChem is close to that in BCC-ESM1, but the PHC is more
473 than 0.1 $^\circ\text{C}$ lower; the aerosol-forcing-sensitivity in UKESM1-0-LL is the strongest
474 ($\sim 1.5 \text{ W mg}^{-1}$) but not the PHC bias. Therefore, the aerosol-forcing-sensitivity is not
475 able to explain the different PHC biases among ESMs.

476 As shown in Fig.6b, the sulphate loading differences between the historical and
477 hist-piAer experiments during the PHC period are large among ESMs (the X-axis),
478 which are about 1.5 mg m^{-2} in GFDL-ESM4 but approximately 2.9 mg m^{-2} in EC-
479 Earth3-AerChem. The sulphate loading differences during the PHC period and PHC
480 biases shows a negative correlation: the PHC bias is generally larger in models with
481 higher sulphate loading over this period; the ESMs with similar PHC biases (MPI-ESM,
482 NorESM2, and UKESM1) show similar aerosol loading differences. Therefore, the
483 excessive cooling during the PHC period and the inter-model diversity in ESMs are
484 attributed to the higher aerosol burden in these models.

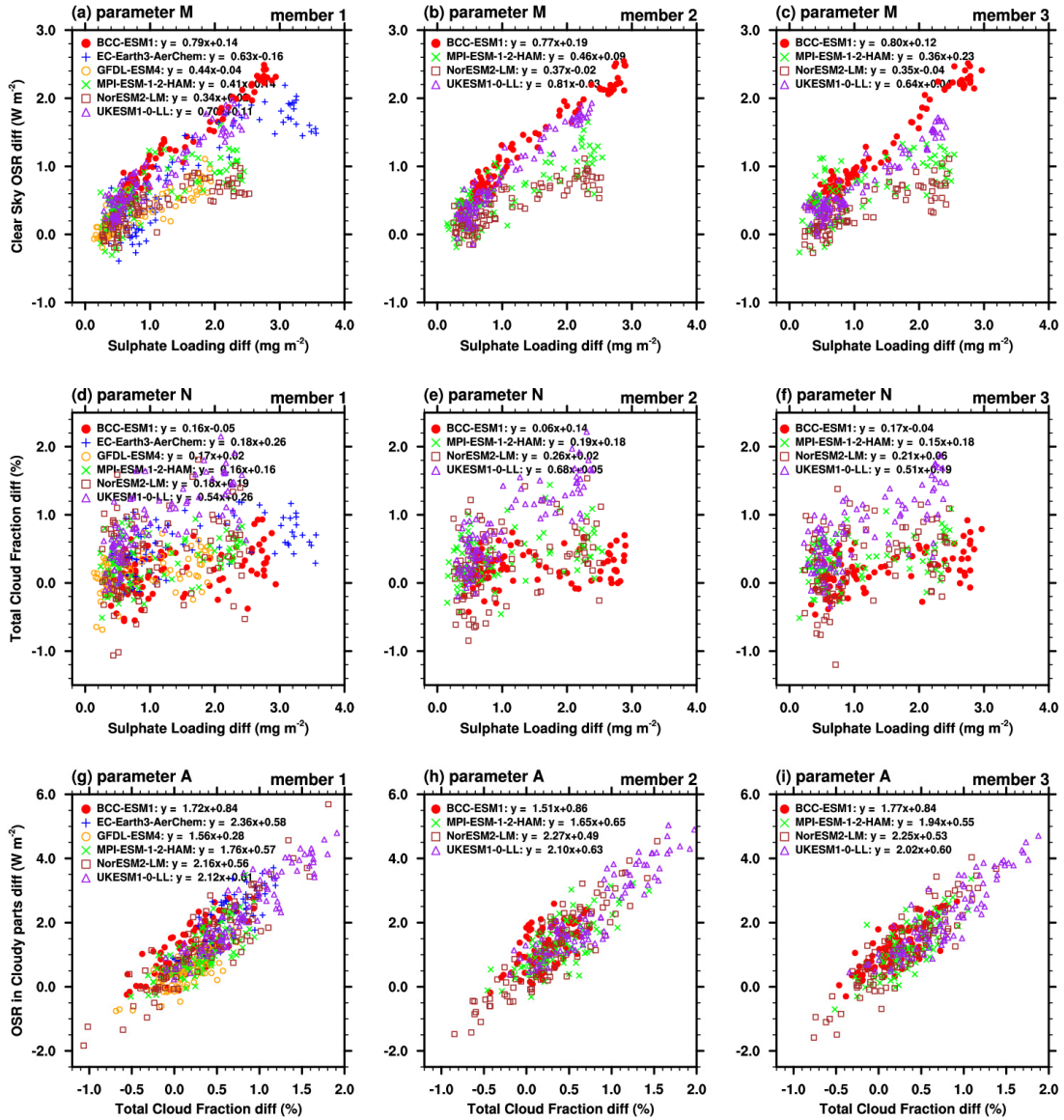
485

486 5. Discussion

487 5.1 The proportions of ARI and ACI

488 Although the aerosol-forcing-sensitivity is not responsible for the anomalous
489 cooling biases in ESMs, it is a good way to identify model differences in the response
490 to aerosol changes. As shown in Fig.5b, there are significant differences in the aerosol-
491 forcing-sensitivity among ESMs. The aerosol-forcing-sensitivity in UKESM1-0-L is
492 almost three times of that in GFDL-ESM4. Due to the uncertainties in physical
493 processes and cloud parameterizations, the dominant component (ARI or ACI) of
494 aerosol-forcing-sensitivity may also vary among ESMs. Here, we separate the different
495 components of the aerosol-forcing-sensitivity in each ESM by the method introduced
496 in the section 2.3 and the Appendix. Sulphate loading is used as a proxy of aerosol
497 amount for all aerosol components in the quantification of the total effect because of its
498 dominant contribution to anthropogenic aerosol load during this period and its
499 covariation with the other aerosol species.

500



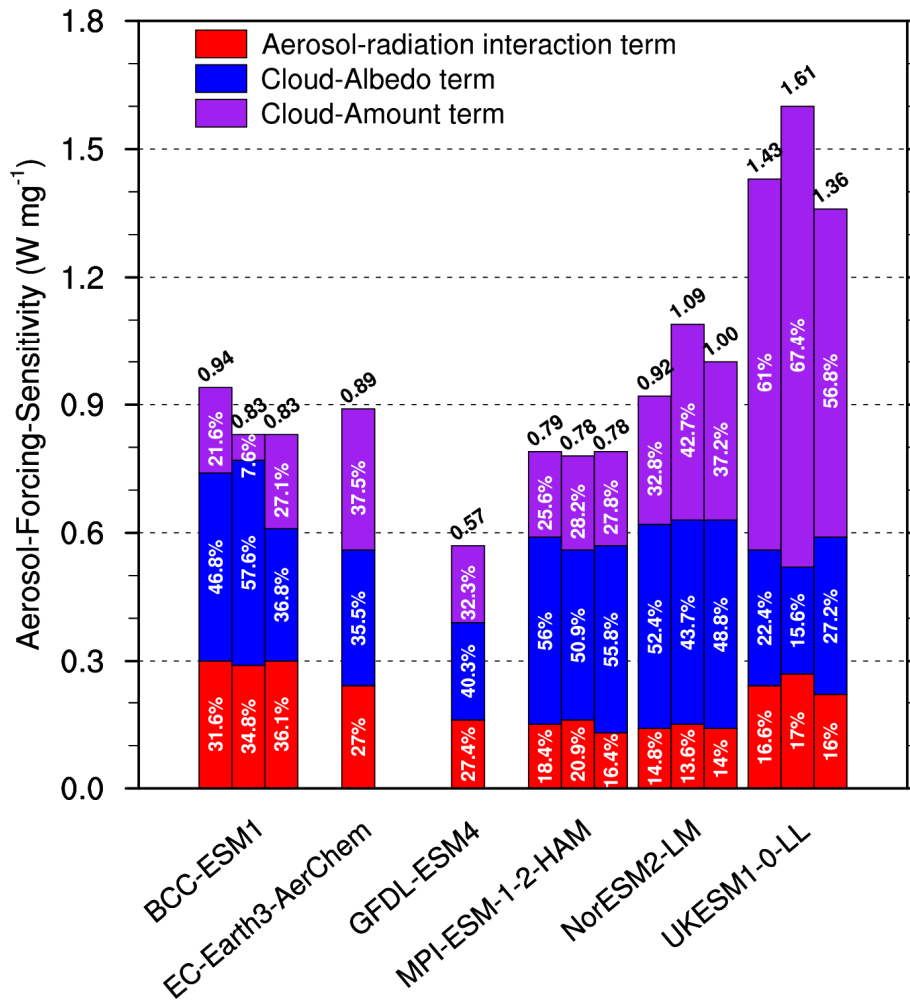
501
 502 **Figure 7.** Annual mean differences between the historical and hist-piAer simulations in the ESM
 503 members during 1900 to 1990 period for (a-c) sulphate loading (mg m^{-2}) versus clear-sky OSR (OSR_{clr} ,
 504 W m^{-2}), (d-f) sulphate loading versus total cloud fraction (%), and (g-i) total cloud fraction versus OSR
 505 in cloudy parts (W m^{-2}). Slopes of the linear fitting equations from the top row to the bottom row refer
 506 to the parameters M, N, and A, respectively.

507

508 The ARI can be ~~generally parameterized as approximated to~~ $(1 - \text{CLT}_{\text{hist}}/100) \cdot M$,
 509 where CLT_{hist} is cloud amount in the historical simulation and parameter M is a
 510 measure of the strength of aerosol-radiation interactions ($\Delta \text{OSR}_{\text{clr}} / \Delta \text{loadSO}_4$).
 511 Parameter M varies widely from about 0.35 W mg^{-1} in NorESM2-LM to about 0.79 W

512 mg^{-1} in BCC-ESM1 (captions in Fig.7a-7c). Since parameter M does not change much
 513 among ensemble members in each ESM, their ARI is similar across members. That is,
 514 the impact of internal climate variability on the ARI is relatively small, which is
 515 consistent with the quantitative analysis in Fig.8 (Red bars).

516



517

518 **Figure 8.** Total aerosol-forcing-sensitivity from each member in ESMs. The number marked on the top
 519 is the total aerosol-forcing-sensitivity. Partition of aerosol-radiation interaction term, cloud-albedo term,
 520 and cloud-amount term are marked in the corresponding color bars. Unit: W mg^{-1} . Where multiple
 521 realizations are available for a model, a bar is shown for each member.

522

523 The ACI can be estimated from the difference between the aerosol-forcing-
 524 sensitivity and the ARI. The proportion of the aerosol-forcing-sensitivity arising from

525 the ACI is higher than 64% in all ESMs (Fig.8). The inter-model variation of the ACI
526 (0.37 W mg^{-1}) is much larger than that for the ARI (0.09 W mg^{-1}). For example, the ACI
527 in UKESM1-0-LL ($\sim 1.2 \text{ W mg}^{-1}$) is higher than all the others and is about three times
528 of that in GFDL-ESM4 (0.41 W mg^{-1}). This demonstrates that differences in the
529 aerosol-forcing-sensitivity across the ESMs are dominated by the differences in their
530 individual representation of ACI. [Chen et al. \(2014\) also suggested that ACI is the main](#)
531 [contribution to the Aerosol radiative forcing uncertainty and the response of marine](#)
532 [clouds to aerosol changes is paramount.](#) The intra-model variations in the ACI are also
533 larger than that for the ARI. That is because the intra-model variations of the ACI are
534 influenced by the effects of climate system internal variability on aerosol-induced cloud
535 microphysics, with cloud radiative properties and cloud lifetimes varying regionally.
536 The intra-model variations are also attributable to the differences in atmospheric
537 circulation among different ensemble members, which may affect the geographical
538 distributions of aerosols and clouds and lead to a different magnitude of interactions.

539 The quantitative analysis in Fig.8 also indicates that ESMs with similar aerosol-
540 forcing-sensitivity may have different contributions from ARI and ACI. The aerosol-
541 forcing-sensitivity is similar in BCC-ESM1, EC-Earth3-AerChem, MPI-ESM-1-2-
542 HAM and NorESM2-LM, but the fractional contribution from the ACI is the largest in
543 NorESM2-LM and its ARI is less than half of that in BCC-ESM1. Generally, BCC-
544 ESM1 has the largest fractional ARI contribution (34%), whereas NorESM2-LM has
545 the largest fraction of ACI contribution (86%).

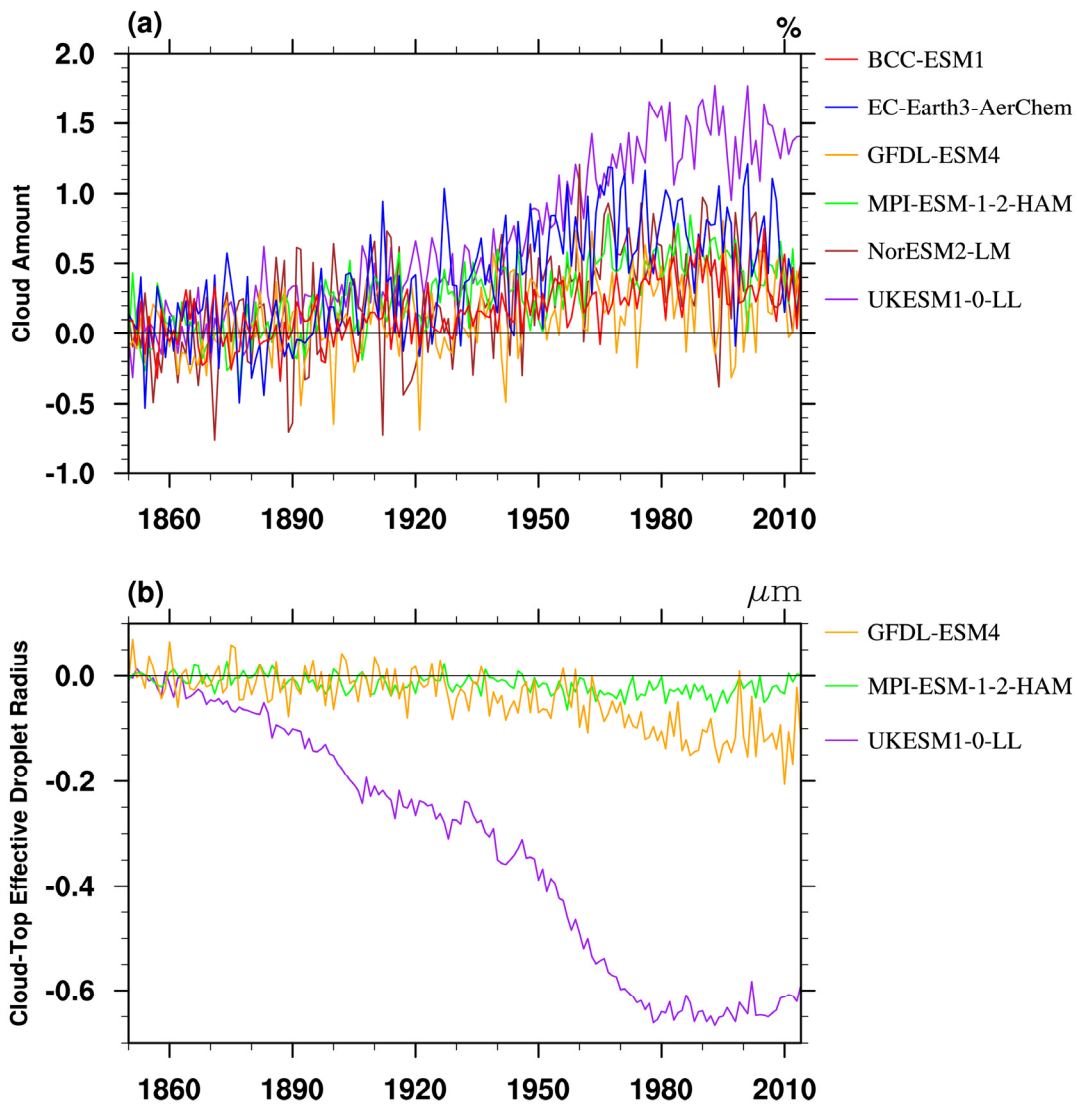
546

547 **5.2 The proportions of cloud-amount and cloud-albedo terms**

548 Our ACI metric includes several mechanisms by which aerosols can alter cloud
549 properties. This includes the cloud-albedo effects (or 'Twomey' effect), referred to as
550 the radiative forcing part of ACI, and effects of aerosols on the macroscopic properties
551 of clouds (for example, cloud extent and lifetime), referred to as the adjustments part
552 of ACI. However, it is complicated to separate these two parts of ACI directly using
553 available CMIP6 diagnostics, because the former is most accurately defined as a change

554 in cloud albedo with all other cloud properties held constant (i.e., a change in cloud-
 555 droplet number concentration only), whilst the latter allows cloud properties to respond.

556



557

558

559 **Figure 9** (a) Evolutions of global mean cloud amount differences between the historical and hist-piAer

560 simulations in ensemble mean for each ESM, units: %. (b) is the same as (a), but for cloud-top

561 effective droplet radius (r_{eff} , μm). The r_{eff} data is only available for GFDL-ESM4, MPI-ESM-1-2-HAM,

562 and UKESM1-0-LL.

563

564 Figure 9 shows the evolution of global-mean differences in total cloud amount

565 (ΔCLT) and cloud-top effective droplet radius (Δr_{eff}) between the historical and hist-

566 piAer experiments. The ΔCLT and Δr_{eff} in UKESM1-0-LL are the largest and highly
567 correlated with each other (with a correlation coefficient of -0.92 during the 1900 to
568 1990 period). For the other two ESMs for which Δr_{eff} was archived, the correlation
569 coefficient is -0.40 for MPI-ESM-1-2-HAM and insignificant for GFDL-ESM4 (-0.09).
570 The ΔCLT and Δr_{eff} differences are smaller in MPI-ESM-1-2-HAM and GFDL-ESM4
571 than in UKESM1-0-LL, especially for the Δr_{eff} differences. Δr_{eff} is generally related to
572 the cloud-optical depth and cloud water path, and ΔCLT is related to adjustments in
573 cloud cover due to ACI. Therefore, the radiative forcing part and adjustments part of
574 ACI may be closely coupled in UKESM1-0-LL and are hard to separate statistically.
575 The strong correlation between cloud amount and r_{eff} response in UKESM1-0-LL
576 indicates that this model is sensitive to aerosol-cloud interactions, which ~~is~~ likely ~~to~~
577 contributes to it having the strongest aerosol-forcing-sensitivity and intra-model spread
578 of all the CMIP6 models (Fig.5c). MPI-ESM-1-2-HAM and UKESM1-0-LL have
579 similar ensemble mean PHC biases and close sulphate burden, but the aerosol-forcing-
580 sensitivity differences in UKESM1-0-LL is almost twice of that in MPI-ESM-1-2-
581 HAM (Fig.5). That is, the overestimated sulphate burden dominates the PHC biases,
582 but the ACI sensitivity may partly affect the amplitude and uncertainty ranges of PHC
583 biases.

584 Despite of the closely coupled radiative forcing part and adjustments part of ACI
585 in UKESM1-0-LL, it is still possible to split the ACI into a part that is correlated with
586 cloud amount differences and a residual term. This can be done statistically by
587 regressing-out the approximate linear dependence of the differences between historical
588 and hist-piAer simulations of the cloudy part of OSR (OSRcld_p) on cloud fraction in
589 each ESM (parameter A in Fig.7g-7i). We call the degree of linear correlation of
590 ΔOSRcld_p with ΔCLT the "cloud-amount term", and the residual will be referred to
591 as the "cloud-albedo term". However, we reiterate that the so-called "cloud-amount
592 term" may also include changes in the reflectivity of clouds if these are correlated with
593 changes in cloud amount. Similarly, the cloud-albedo term will contain any sources of
594 cloud amount changes which have not been removed by linearly regressing OSRcld_p

595 against cloud amount. As such, we do not intend this nomenclature to indicate a precise
596 separation of the radiative forcing part and adjustments part of ACI. Our decomposition
597 allows first order assessment of these terms from historical simulations without the need
598 for extra simulations or calls, and also allows estimates from observations and
599 intermodel comparisons.

600 As described in the section 2.3 and the Appendix, the cloud-amount term is
601 sensitive to two parameters: the cloud amount response (parameter N in Fig.7d-7f) and
602 the sensitivity of OSR reflected from clouds to cloud amount changes (parameter A,
603 Fig.7g-7i). As shown in Fig.8, UKESM1-0-LL has the largest contribution of the cloud-
604 amount term to aerosol-forcing-sensitivity (62%, 0.91W mg^{-1}); the cloud-amount term
605 is the smallest in GFDL-ESM4 ($\sim 0.18\text{W mg}^{-1}$). The cloud-albedo term is defined to be
606 linearly independent of cloud-amount changes (adjustments). For the CMIP6 ESMs, it
607 can only be estimated as the residual after subtracting the cloud-amount term from the
608 ACI. The cloud-albedo term is similar in BCC-ESM1, MPI-ESM-1-2-HAM, and
609 NorESM2-LM. The inter-model variation for the cloud-amount term is about twice of
610 that for the cloud-albedo term (0.29W/mg v.s. 0.16W/mg). That is, the variations of
611 cloud-amount term are the major source of inter-model ACI (and the aerosol-forcing-
612 sensitivity) differences between ESMs. Therefore, difference in the cloud-amount
613 terms, across the ESMs, dominates the uncertainties in the aerosol-forcing-sensitivity.

614 Note that, ~~neither do~~ our definitions do not correspond to the effects measured by
615 using multiple calls to the radiation scheme of a model, with and without aerosols,
616 which measure instantaneous radiative effects; multiple calls give a measure of the fast
617 response of clouds to aerosol perturbations in a fixed thermodynamic and dynamical
618 background, allowing for a clear separation between ACI and rapid adjustments (e.g.,
619 Bellouin et al., 2013). This differs from aerosol forcing diagnosed by differencing
620 climate projections with different aerosol forcings, which include the slow effects of
621 other feedbacks. For example, differences in climate forcings can lead to different SST
622 patterns, which in turn alter the location and characteristics of clouds. Despite these
623 differences, an advantage of our classification is that it provides a possible method for

624 model evaluation since the variables used are also, in principle, available from the
625 observations.

626

627 6. Conclusion

628 This study focuses on the reproduction of historical surface air temperature
629 anomalies in six CMIP6 ESMs. The ESMs systematically underestimate TAS
630 anomalies relative to 1850 to 1900 in the NH midlatitudes, especially from 1960 to
631 1990, the "pot-hole" cooling (PHC) period. ~~In the global mean, the excessive cooling~~
632 ~~in models is more pronounced at the surface, which is distinct from the response to~~
633 ~~greenhouse gases that preferentially heat the tropical upper troposphere.~~ Previous
634 studies suggested that aerosol cooling is too strong in many CMIP6 models. Our study
635 more specifically found that the PHC is concurrent in time and space with
636 anthropogenic SO₂ emissions, which rapidly increase in the PHC period in NH. Models
637 with larger aerosol burdens have larger PHC biases. The primary role of aerosol
638 emissions in these biases is further supported by the differences between ESMs and the
639 lower-complexity models with prescribed aerosol.

640 Differences between historical simulations and simulations with aerosol emissions
641 fixed at their preindustrial levels (hist-piAer) are used to isolate the impacts of industrial
642 aerosol emission. We propose that the overestimated aerosol concentrations ~~and~~
643 ~~aerosol forcing sensitivity~~ in the ESMs are responsible ~~account~~ for the spurious drop
644 in TAS in the mid-twentieth century, rather than a high sensitivity of the models to
645 aerosol forcing.

646 Although the aerosol-forcing-sensitivity differences in ESMs cannot explain the
647 PHC biases, it is a good measurement of aerosol effects that can be used to explore
648 structural differences between models. A simple metric is derived for determining the
649 dominant contribution to the aerosol-forcing-sensitivity in any specific model: ARI or
650 ACI. ~~The ARI has a slight intra-model variation.~~ The ACI accounts for more than 64%
651 of the aerosol-forcing-sensitivity in all analyzed ESMs. The considerable inter-model

652 variation in the aerosol-forcing-sensitivity is mainly attributable to the uncertainty in
653 the ACI within models. The ACI can be further decomposed into a cloud-amount term
654 and a cloud-albedo term. The cloud-amount term is found to be the major source of
655 inter-model diversity of ACI. Considering the crucial role of cloud properties on the
656 inter-model spread in aerosol-forcing-sensitivity, the aerosol-cloud interactions should
657 be a focus in development of aerosol schemes within ESMs.

658

659

660 **Appendix: Decomposition of the Aerosol-radiation interaction and aerosol-cloud**
661 **interaction**

662 Considering the dominant role of sulphate aerosol on anthropogenic aerosol
663 forcing, we use the sulphate loading (loadSO4) as a proxy for all aerosol in our analysis.
664 The aerosol-forcing-sensitivity (as determined by the difference between the historical
665 and hist-piAer experiments) is estimated by the all-sky OSR differences per sulfate
666 burden unit ($\Delta OSR / \Delta loadSO4$) and it is the combination of OSR differences in the
667 clear-sky parts ($\Delta OSR_{clr_p} / \Delta loadSO4$) and the cloudy parts ($\Delta OSR_{cld_p} / \Delta$
668 $loadSO4$):

$$669 \quad \Delta OSR / \Delta loadSO4 = \Delta OSR_{clr_p} / \Delta loadSO4 + \Delta OSR_{cld_p} / \Delta loadSO4.$$

670 (A1)

671 The OSR_{clr_p} for a particular experiment can be calculated as:

$$672 \quad OSR_{clr_p} = (1-CLT/100.) * OSR_{clr}, \quad (A2)$$

673 where CLT is the total cloud amount (unit: %), and OSR_{clr} is the OSR assuming all
674 clear sky (unit: W/m^2). The cloud amount changes (ΔCLT) will modify the proportion
675 of clear-sky and then affect the OSR changes attributed to the clear-sky part by covering
676 or uncovering aerosols in clear sky. Therefore, based on equation (A2), $\Delta OSR_{clr_p} / \Delta$
677 $loadSO4$ can be decomposed into the OSR_{clr} -response ($\Delta OSR_{clr} / \Delta loadSO4$) and
678 CLT-response ($\Delta CLT / \Delta loadSO4$):

$$679 \quad \Delta OSR_{clr_p} / \Delta loadSO4 = (1-CLT_{hist}/100.) * \Delta OSR_{clr} / \Delta loadSO4$$
$$680 \quad - OSR_{clr_hist} / 100 * \Delta CLT / \Delta loadSO4 + residual_clrp$$
$$681 \quad = (1-CLT_{hist}/100.) * M - OSR_{clr_hist} / 100 * N + residual_clr, \quad (A3)$$

682 where CLT_{hist} and OSR_{clr_hist} are the mean CLT and OSR_{clr} in the historical
683 experiment. $Residual_clr$ is the residual term that is non-linear in ΔOSR_{clr} and ΔCLT .
684 The parameter $M = \Delta OSR_{clr} / \Delta loadSO4$ is related to strength of aerosol-radiation
685 interaction and can be estimated by linear fitting of ΔOSR_{clr} on $\Delta loadSO4$. The
686 parameter $N = \Delta CLT / \Delta loadSO4$ is related to CLT-response and estimated by linear
687 fitting of ΔCLT on $\Delta loadSO4$. Therefore, the first term on the right-hand side of Eq.
688 (A3), $(1-CLT_{hist}/100.) * M$, corresponds to the aerosol radiative effect; the second term,
689 $- OSR_{clr_hist} / 100 * N$, corresponds to the impact of changes in clear-sky area.

690 The OSR_{cld_p} is the cloudy part of OSR, accounting for the difference between
691 OSR and OSR_{clr_p} . The cloudy part of the OSR differences (ΔOSR_{cld_p}) can be

692 generally estimated as:

$$693 \quad \Delta OSR_{cld_p} = A * \Delta CLT + \text{cloud-albedo relative changes} + \text{residual_cld},$$

694 where the parameter $A = \Delta(OSR - OSR_{clr_p}) / \Delta CLT$ is the sensitivity of the shortwave
695 flux reflected by clouds to changes in cloud amount. The parameter A depends on the
696 baseline cloud albedo (radiative flux per cloud amount unit) and can be estimated by
697 linear fitting of ΔOSR_{cld_p} on ΔCLT . Hence,

$$698 \quad \Delta OSR_{cld_p} / \Delta \text{loadSO4} = A * \Delta CLT / \Delta \text{loadSO4} + \text{cloud-albedo term}$$

$$699 \quad \quad \quad + \text{residual_cld},$$

$$700 \quad \quad \quad = A * N + \text{cloud-albedo term} + \text{residual_cld}, \quad (A4)$$

701

702 where N is the parameter defined above. Therefore, the first term on the right-hand side
703 of equation (A4), $A * N$, corresponds to the impact of cloud amount changes on the cloud
704 radiation; and the cloud-albedo term can be obtained as a residual after subtracting $A * N$
705 from $\Delta OSR_{cld_p} / \Delta \text{loadSO4}$, thereby eliminating any linear dependence of the cloudy-
706 sky shortwave flux response on cloud-amount changes.

707 As with the clear-sky decomposition, *residual_cld* is a possible non-linear term and
708 is assumed to be small. This term cannot in fact be distinguished from the cloud-albedo
709 term, in this analysis: we must therefore accept that cloud-albedo changes could be
710 accompanied by non-linear changes in macroscopic cloud properties (in this
711 framework).

712 The total aerosol-forcing-sensitivity can be measured by substituting the derived
713 values of $\Delta OSR / \Delta \text{loadSO4}$ from both the clear sky (equation A3) and cloudy
714 (equation A4) parts back into equation (A1):

$$715 \quad \Delta OSR / \Delta \text{loadSO4} = (1 - CLT_{hist}/100.) * M - OSR_{clr_hist}/100 * N$$

$$716 \quad \quad \quad + A * N + \text{cloud_albedo_term} + \text{residual}$$

$$717 \quad \quad \quad = (1 - CLT_{hist}/100.) * M + (A - OSR_{clr_hist}/100.) * N$$

$$718 \quad \quad \quad + \text{cloud_albedo_term} + \text{residual_osr}. \quad (A5)$$

719

720 Based on equation (A5), the total aerosol-forcing-sensitivity can therefore be
721 decomposed to the aerosol-radiation interaction term (ARI), $(1 - CLT_{hist}/100.) * M$,
722 cloud-amount term as $(A - OSR_{clr_hist}/100.) * N$ including the impacts of cloud amount
723 changes on aerosol radiation ($-OSR_{clr_hist}/100.*N$) and cloud radiation ($A * N$), and
724 cloud-albedo term (defined as a residual).

725

726

727 **Data Availability.** All the model data can be freely downloaded from the Earth System
728 Federation Grid (ESGF) nodes (<https://esgf-node.llnl.gov/search/cmip6/>). The global
729 historical surface temperature anomalies HadCRUT5 dataset is freely available on
730 <https://www.metoffice.gov.uk/hadobs/hadcrut5/data/current/download.html>.

731

732 **Author contributions**

733 The main ideas were developed by JZ, KF, STT, JPM, and TW. JZ, KF, and STT wrote
734 the original draft, and the results were supervised by LJW, BBB, and DS. All the
735 authors discussed the results and contributed to the final manuscript.

736

737 **Competing interests**

738 The authors declare that they have no conflict of interest.

739

740 **Acknowledgments**

741 This work was supported by The National Key Research and Development Program of
742 China (Grant no. 2018YFE0196000 and 2016YFA0602100). All the AUTHORS were
743 supported by the UK-China Research & Innovation Partnership Fund through the Met
744 Office Climate Science for Service Partnership (CSSP) China as part of the Newton
745 Fund. LJW was supported by the National Environmental Research Council (NERC)
746 “North Atlantic Climate System Integrated Study” (ACSIS) program.

747

748 **Reference**

- 749 Aas, W., Mortier, A., Bowersox, V., Cherian, R., Faluvegi, G., Fagerli, H., Hand, J.,
750 Klimont, Z., Galy-Lacaux, C., Lehmann, C. M. B., Myhre, C. L., Myhre, G., Olivie,
751 D., Sato, K., Quaas, J., Rao, P. S. P., Schulz, M., Shindell, D., Skeie, R. B., Stein,
752 A., Takemura, T., Tsyro, S., Vet, R., and Xu, X.: Global and regional trends of
753 atmospheric sulfur (vol 9, 953, 2019), *Scientific Reports*, 10, 10.1038/s41598-
754 020-62441-w, 2020.
- 755 ALBRECHT, B. A.: Aerosols, Cloud Microphysics, and Fractional Cloudiness,
756 *Science*, 245, 1227-1230, 10.1126/science.245.4923.1227, 1989.
- 757 Bellouin, N., Mann, G. W., Woodhouse, M. T., Johnson, C., Carslaw, K. S., and Dalvi,
758 M.: Impact of the modal aerosol scheme GLOMAP-mode on aerosol forcing in the
759 Hadley Centre Global Environmental Model, *Atmospheric Chemistry and
760 Physics*, 13, 3027-3044, 10.5194/acp-13-3027-2013, 2013.
- 761 Bethke, I., Wang, Y., Counillon, F., Kimmritz, M., Fransner, F., Samuelsen, A.,
762 Langehaug, H. R., Chiu, P.-G., Bentsen, M., Guo, C., Tjiputra, J., Kirkevåg, A.,
763 Olivie, D. J. L., Seland, Ø., Fan, Y., Lawrence, P., Eldevik, T., and Keenlyside,
764 N.: NCC NorCPM1 model output prepared for CMIP6 CMIP, Earth System Grid
765 Federation [dataset], 10.22033/ESGF/CMIP6.10843, 2019.
- 766 Bindoff, N. L., Stott, P. A., AchutaRao, K. M., Allen, M. R., Gillett, N., Gutzler, D.,
767 Hansingo, K., Hegerl, G., et al.: Detection and Attribution of Climate Change:
768 from Global to Regional, in: *Climate Change 2013: The Physical Science Basis.*
769 Contribution of Working Group I to the Fifth Assessment Report of the
770 Intergovernmental Panel on Climate Change [Stocker, T.F., D. Qin, G.-K. Plattner,
771 M. Tignor, S.K. Allen, J. Boschung, A. Nauels, Y. Xia, V. Bex and P.M. Midgley
772 (eds.)]. Cambridge University Press, Cambridge, United Kingdom and New York,
773 NY, USA.
- 774 [Booth, B. B. B., Harris, G. R., Jones, A., Wilcox, L., Hawcroft, M., and Carslaw, K. S.:
775 Comments on “Rethinking the Lower Bound on Aerosol Radiative Forcing”,
776 Journal of Climate, 31, 9407-9412, 10.1175/jcli-d-17-0369.1, 2018.](#)
- 777 [Carslaw, K. S., Lee, L. A., Reddington, C. L., Pringle, K. J., Rap, A., Forster, P. M.,
778 Mann, G. W., Spracklen, D. V., Woodhouse, M. T., Regayre, L. A., and Pierce, J.
779 R.: Large contribution of natural aerosols to uncertainty in indirect forcing, Nature,
780 503, 67-71, 10.1038/nature12674, 2013.](#)
- 781 Charlson, R. J., Langner, J., and Rodhe, H.: Sulphate aerosol and climate, *Nature*, 348,
782 22-22, 10.1038/348022a0, 1990.
- 783 [Chen, Y.-C., Christensen, M. W., Stephens, G. L., and Seinfeld, J. H.: Satellite-based
784 estimate of global aerosol–cloud radiative forcing by marine warm clouds, Nat.
785 Geosci., 7, 643-646, 10.1038/ngeo2214, 2014.](#)
- 786 [Christensen, M. W., Neubauer, D., Poulsen, C. A., Thomas, G. E., McGarragh, G. R.,
787 Povey, A. C., Proud, S. R., and Grainger, R. G.: Unveiling aerosol-cloud
788 interactions - Part 1: Cloud contamination in satellite products enhances the
789 aerosol indirect forcing estimate, Atmospheric Chemistry and Physics, 17, 13151-
790 13164, 10.5194/acp-17-13151-2017, 2017.](#)

791 Collins, W., Lamarque, J.-F., Schulz, M., Boucher, O., Eyring, V., Hegglin, M.,
792 Maycock, A., Myhre, G., Prather, M., Shindell, D., and Smith, S.: AerChemMIP:
793 Quantifying the effects of chemistry and aerosols in CMIP6, *Geoscientific Model*
794 *Development*, 10, 585-607, 10.5194/gmd-10-585-2017, 2017.

795 Collins, W. J., Fry, M. M., Yu, H., Fuglestvedt, J. S., Shindell, D. T., and West, J. J.:
796 Global and regional temperature-change potentials for near-term climate forcers,
797 *Atmospheric Chemistry and Physics*, 13, 2471-2485, 10.5194/acp-13-2471-2013,
798 2013.

799 Dittus, A. J., Hawkins, E., Wilcox, L. J., Sutton, R. T., Smith, C. J., Andrews, M. B.,
800 and Forster, P. M.: Sensitivity of Historical Climate Simulations to Uncertain
801 Aerosol Forcing, *Geophysical Research Letters*, 47, e2019GL085806,
802 10.1029/2019gl085806, 2020.

803 Döscher, R., Acosta, M., Alessandri, A., Anthoni, P., Arneth, A., Arsouze, T.,
804 Bergmann, T., Bernadello, R., Bousetta, S., Caron, L.-P., Carver, G., Castrillo, M.,
805 Catalano, F., Cvijanovic, I., Davini, P., Dekker, E., Doblus-Reyes, F. J., Docquier,
806 D., Echevarria, P., Fladrich, U., Fuentes-Franco, R., Gröger, M., v. Hardenberg,
807 J., Hieronymus, J., Karami, M. P., Keskinen, J.-P., Koenigk, T., Makkonen, R.,
808 Massonnet, F., Ménégoz, M., Miller, P. A., Moreno-Chamarro, E., Nieradzick, L.,
809 van Noije, T., Nolan, P., O'Donnell, D., Ollinaho, P., van den Oord, G., Ortega,
810 P., Prims, O. T., Ramos, A., Reerink, T., Rousset, C., Ruprich-Robert, Y., Le Sager,
811 P., Schmith, T., Schrödner, R., Serva, F., Sicardi, V., Sloth Madsen, M., Smith, B.,
812 Tian, T., Tourigny, E., Uotila, P., Vancoppenolle, M., Wang, S., Wårlind, D.,
813 Willén, U., Wyser, K., Yang, S., Yepes-Arbós, X., and Zhang, Q.: The EC-Earth3
814 Earth System Model for the Climate Model Intercomparison Project 6, *Geosci.*
815 *Model Dev. Discuss.* [preprint], <https://doi.org/10.5194/gmd-2020-446>, in review,
816 2021.

817 Dunne, J. P., Horowitz, L. W., Adcroft, A. J., Ginoux, P., Held, I. M., John, J. G.,
818 Krasting, J. P., Malyshev, S., Naik, V., Paulot, F., Shevliakova, E., Stock, C. A.,
819 Zadeh, N., Balaji, V., Blanton, C., Dunne, K. A., Dupuis, C., Durachta, J., Dussin,
820 R., Gauthier, P. P. G., Griffies, S. M., Guo, H., Hallberg, R. W., Harrison, M., He,
821 J., Hurlin, W., McHugh, C., Menzel, R., Milly, P. C. D., Nikonov, S., Paynter, D.
822 J., Ploshay, J., Radhakrishnan, A., Rand, K., Reichl, B. G., Robinson, T.,
823 Schwarzkopf, D. M., Sentman, L. T., Underwood, S., Vahlenkamp, H., Winton,
824 M., Wittenberg, A. T., Wyman, B., Zeng, Y., and Zhao, M.: The GFDL Earth
825 System Model Version 4.1 (GFDL-ESM 4.1): Overall Coupled Model Description
826 and Simulation Characteristics, *J. Adv. Model. Earth Syst.*, 12,
827 10.1029/2019ms002015, 2020.

828 Eyring, V., Bony, S., Meehl, G. A., Senior, C. A., Stevens, B., Stouffer, R. J., and
829 Taylor, K. E.: Overview of the Coupled Model Intercomparison Project Phase 6
830 (CMIP6) experimental design and organization, *Geosci. Model Dev.*, 9, 1937-
831 1958, 10.5194/gmd-9-1937-2016, 2016.

832 Flynn, C. M. and Mauritsen, T.: On the climate sensitivity and historical warming
833 evolution in recent coupled model ensembles, *Atmos. Chem. Phys.*, 20, 7829-7842,
834 10.5194/acp-20-7829-2020, 2020.

835 Gillett, N. P., Shiogama, H., Funke, B., Hegerl, G., Knutti, R., Matthes, K., Santer, B.
836 D., Stone, D., and Tebaldi, C.: The Detection and Attribution Model
837 Intercomparison Project (DAMIP v1.0) contribution to CMIP6, *Geosci. Model*
838 *Dev.*, 9, 3685-3697, 10.5194/gmd-9-3685-2016, 2016.

839 Held, I. M., Guo, H., Adcroft, A., Dunne, J. P., Horowitz, L. W., Krasting, J.,
840 Shevliakova, E., Winton, M., Zhao, M., Bushuk, M., Wittenberg, A. T., Wyman,
841 B., Xiang, B., Zhang, R., Anderson, W., Balaji, V., Donner, L., Dunne, K.,
842 Durachta, J., Gauthier, P. P. G., Ginoux, P., Golaz, J. C., Griffies, S. M., Hallberg,
843 R., Harris, L., Harrison, M., Hurlin, W., John, J., Lin, P., Lin, S. J., Malyshev, S.,
844 Menzel, R., Milly, P. C. D., Ming, Y., Naik, V., Paynter, D., Paulot, F.,
845 Rammamswamy, V., Reichl, B., Robinson, T., Rosati, A., Seman, C., Silvers, L. G.,
846 Underwood, S., and Zadeh, N.: Structure and Performance of GFDL's CM4.0
847 Climate Model, *J. Adv. Model. Earth Syst.*, 11, 3691-3727,
848 10.1029/2019ms001829, 2019.

849 [Hoesly, R. M. et al. Historical \(1750–2014\) anthropogenic emissions of reactive gases](#)
850 [and aerosols from the Community Emissions Data System \(CEDS\). *Geosci. Model*](#)
851 [Dev. 11, 369–408 \(2018\).](#)

852 Kennedy, J. J., Rayner, N. A., Atkinson, C. P., and Killick, R. E.: An Ensemble Data
853 Set of Sea Surface Temperature Change From 1850: The Met Office Hadley
854 Centre HadSST.4.0.0.0 Data Set, *Journal of Geophysical Research-Atmospheres*,
855 124, 7719-7763, 10.1029/2018jd029867, 2019.

856 Lohmann, U. and Feichter, J.: Global indirect aerosol effects: a review, *Atmospheric*
857 *Chemistry and Physics*, 5, 715-737, 10.5194/acp-5-715-2005, 2005.

858 Manktelow, P. T., Mann, G. W., Carslaw, K. S., Spracklen, D. V., and Chipperfield, M.
859 P.: Regional and global trends in sulfate aerosol since the 1980s, *Geophysical*
860 *Research Letters*, 34, 10.1029/2006gl028668, 2007.

861 Mauritsen, T., Bader, J., Becker, T., Behrens, J., Bittner, M., Brokopf, R., Brovkin, V.,
862 Claussen, M., Crueger, T., Esch, M., Fast, I., Fiedler, S., Flaeschner, D., Gayler,
863 V., Giorgetta, M., Goll, D. S., Haak, H., Hagemann, S., Hedemann, C.,
864 Hohengegger, C., Ilyina, T., Jahns, T., Jimenez-de-la-Cuesta, D., Jungclaus, J.,
865 Kleinen, T., Kloster, S., Kracher, D., Kinne, S., Kleberg, D., Lasslop, G.,
866 Kornblueh, L., Marotzke, J., Matei, D., Meraner, K., Mikolajewicz, U., Modali,
867 K., Moebis, B., Muellner, W. A., Nabel, J. E. M. S., Nam, C. C. W., Notz, D.,
868 Nyawira, S.-S., Paulsen, H., Peters, K., Pincus, R., Pohlmann, H., Pongratz, J.,
869 Popp, M., Raddatz, T. J., Rast, S., Redler, R., Reick, C. H., Rohrschneider, T.,
870 Schemann, V., Schmidt, H., Schnur, R., Schulzweida, U., Six, K. D., Stein, L.,
871 Stemmler, I., Stevens, B., von Storch, J.-S., Tian, F., Voigt, A., Vrese, P., Wieners,
872 K.-H., Wilkenskjaeld, S., Winkler, A., and Roeckner, E.: Developments in the MPI-
873 M Earth System Model version 1.2 (MPI-ESM1.2) and Its Response to Increasing
874 CO₂, *J. Adv. Model. Earth Syst.*, 11, 998-1038, 10.1029/2018ms001400, 2019.

875 Meehl, G. A., Senior, C. A., Eyring, V., Flato, G., Lamarque, J.-F., Stouffer, R. J.,
876 Taylor, K. E., and Schlund, M.: Context for interpreting equilibrium climate
877 sensitivity and transient climate response from the CMIP6 Earth system models,
878 *Science Advances*, 6, 10.1126/sciadv.aba1981, 2020.

879 Mitchell, J. F. B., Johns, T. C., Gregory, J. M., and Tett, S. F. B.: Climate response to
880 increasing levels of greenhouse gases and sulphate aerosols, *Nature*, 376, 501-504,
881 10.1038/376501a0, 1995.

882 Morice, C. P., Kennedy, J. J., Rayner, N. A., Winn, J. P., Hogan, E., Killick, R. E.,
883 Dunn, R. J. H., Osborn, T. J., Jones, P. D., and Simpson, I. R.: An Updated
884 Assessment of Near-Surface Temperature Change From 1850: The HadCRUT5
885 Data Set, *Journal of Geophysical Research-Atmospheres*, 126,
886 10.1029/2019jd032361, 2021.

887 Myhre, G., D. Shindell, F.-M. Bréon, W. Collins, J. Fuglestedt, J. Huang, D. Koch, J.-
888 F. Lamarque, D. Lee, B. Mendoza, T. Nakajima, A. Robock, G. Stephens, T.
889 Takemura and H. Zhang: Anthropogenic and Natural Radiative Forcing, in:
890 *Climate Change 2013: The Physical Science Basis. Contribution of Working*
891 *Group I to the Fifth Assessment Report of the Intergovernmental Panel on Climate*
892 *Change* [Stocker, T.F., D. Qin, G.-K. Plattner, M. Tignor, S.K. Allen, J. Boschung,
893 A. Nauels, Y. Xia, V. Bex and P.M. Midgley (eds.)]. Cambridge University Press,
894 Cambridge, United Kingdom and New York, NY, USA.

895 [Neubauer, D., Christensen, M. W., Poulsen, C. A., and Lohmann, U.: Unveiling](#)
896 [aerosol-cloud interactions - Part 2: Minimising the effects of aerosol swelling and](#)
897 [wet scavenging in ECHAM6-HAM2 for comparison to satellite data, *Atmospheric*](#)
898 [*Chemistry and Physics*, 17, 13165-13185, 10.5194/acp-17-13165-2017, 2017.](#)

899 [Neubauer, D., Ferrachat, S., Siegenthaler-Le Drian, C., Stoll, J., Folini, D. S., Tegen, I.,](#)
900 [Wiener, K.-H., Mauritsen, T., Stemmler, I., Barthel, S., Bey, I., Daskalakis, N.,](#)
901 [Heinold, B., Kokkola, H., Partridge, D., Rast, S., Schmidt, H., Schutgens, N.,](#)
902 [Stanelle, T., Stier, P., Watson-Parris, D., and Lohmann, U.: HAMMOZ-](#)
903 [Consortium MPI-ESM1.2-HAM model output prepared for CMIP6 AerChemMIP,](#)
904 [Earth System Grid Federation \[dataset\], 10.22033/ESGF/CMIP6.1621, 2019.](#)

905 Noije, T., Bergman, T., Sager, P., O'Donnell, D., Makkonen, R., Gonçalves-Ageitos,
906 M., Döscher, R., Fladrich, U., Hardenberg, J., Keskinen, J.-P., Korhonen, H.,
907 Laakso, A., Myriokefalitakis, S., Ollinaho, P., Pérez García-Pando, C., Reerink,
908 T., Schrödner, R., Wyser, K., and Yang, S.: EC-Earth3-AerChem, a global climate
909 model with interactive aerosols and atmospheric chemistry participating in CMIP6,
910 10.5194/gmd-2020-413, 2020.

911 Osborn, T. J., Jones, P. D., Lister, D. H., Morice, C. P., Simpson, I. R., Winn, J. P.,
912 Hogan, E., and Harris, I. C.: Land Surface Air Temperature Variations Across the
913 Globe Updated to 2019: The CRUTEM5 Data Set, *Journal of Geophysical*
914 *Research: Atmospheres*, 126, e2019JD032352,
915 <https://doi.org/10.1029/2019JD032352>, 2021.

916 Ramanathan, V. and Feng, Y.: Air Pollution, Greenhouse Gases and Climate Change:
917 Global and Regional Perspectives, *Atmospheric Environment*, 43, 37-50,
918 10.1016/j.atmosenv.2008.09.063, 2009.

919 Seland, Ø., Bentsen, M., Olivíe, D., Toniazzo, T., Gjermundsen, A., Graff, L. S.,
920 Debernard, J. B., Gupta, A. K., He, Y.-C., Kirkevåg, A., Schwinger, J., Tjiputra,
921 J., Aas, K. S., Bethke, I., Fan, Y., Griesfeller, J., Grini, A., Guo, C., Ilicak, M.,
922 Karset, I. H. H., Landgren, O., Liakka, J., Moseid, K. O., Nummelin, A.,

923 Spensberger, C., Tang, H., Zhang, Z., Heinze, C., Iversen, T., and Schulz, M.:
924 Overview of the Norwegian Earth System Model (NorESM2) and key climate
925 response of CMIP6 DECK, historical, and scenario simulations, *Geosci. Model*
926 *Dev.*, 13, 6165–6200, <https://doi.org/10.5194/gmd-13-6165-2020>, 2020.

927 Sellar, A. A., Jones, C. G., Mulcahy, J. P., Tang, Y., Yool, A., Wiltshire, A., O'Connor,
928 F. M., Stringer, M., Hill, R., Palmieri, J., Woodward, S., de Mora, L., Kuhlbrodt,
929 T., Rumbold, S. T., Kelley, D. I., Ellis, R., Johnson, C. E., Walton, J., Abraham,
930 N. L., Andrews, M. B., Andrews, T., Archibald, A. T., Berthou, S., Burke, E.,
931 Blockley, E., Carslaw, K., Dalvi, M., Edwards, J., Folberth, G. A., Gedney, N.,
932 Griffiths, P. T., Harper, A. B., Hendry, M. A., Hewitt, A. J., Johnson, B., Jones,
933 A., Jones, C. D., Keeble, J., Liddicoat, S., Morgenstern, O., Parker, R. J., Predoi,
934 V., Robertson, E., Siahahan, A., Smith, R. S., Swaminathan, R., Woodhouse, M. T.,
935 Zeng, G., and Zerroukat, M.: UKESM1: Description and Evaluation of the UK
936 Earth System Model, *J. Adv. Model. Earth Syst.*, 11, 4513-4558,
937 [10.1029/2019ms001739](https://doi.org/10.1029/2019ms001739), 2019.

938 Shindell, D. and Faluvegi, G.: Climate response to regional radiative forcing during the
939 twentieth century, *Nat. Geosci.*, 2, 294-300, [10.1038/ngeo473](https://doi.org/10.1038/ngeo473), 2009.

940 [Smith, C. J., Kramer, R. J., Myhre, G., Alterskjaer, K., Collins, W., Sima, A., Boucher,](#)
941 [O., Dufresne, J.-L., Nabat, P., Michou, M., Yukimoto, S., Cole, J., Paynter, D.,](#)
942 [Shiogama, H., O'Connor, F. M., Robertson, E., Wiltshire, A., Andrews, T.,](#)
943 [Hannay, C., Miller, R., Nazarenko, L., Kirkevag, A., Olivie, D., Fiedler, S.,](#)
944 [Lewinschal, A., Mackallah, C., Dix, M., Pincus, R., and Forster, P. M.: Effective](#)
945 [radiative forcing and adjustments in CMIP6 models, *Atmospheric Chemistry and*](#)
946 [*Physics*, 20, 9591-9618, \[10.5194/acp-20-9591-2020\]\(https://doi.org/10.5194/acp-20-9591-2020\), 2020.](#)

947 Stevens, B., Fiedler, S., Kinne, S., Peters, K., Rast, S., Muesse, J., Smith, S. J., and
948 Mauritsen, T.: MACv2-SP: a parameterization of anthropogenic aerosol optical
949 properties and an associated Twomey effect for use in CMIP6, *Geoscientific*
950 *Model Development*, 10, 433-452, [10.5194/gmd-10-433-2017](https://doi.org/10.5194/gmd-10-433-2017), 2017.

951 Thorne, P. W., Lanzante, J. R., Peterson, T. C., Seidel, D. J., and Shine, K. P.:
952 Tropospheric temperature trends: history of an ongoing controversy, *Wiley*
953 *Interdisciplinary Reviews-Climate Change*, 2, 66-88, [10.1002/wcc.80](https://doi.org/10.1002/wcc.80), 2011.

954 [Wang, Z., Lin, L., Xu, Y., Che, H., Zhang, X., Zhang, H., Dong, W., Wang, C., Gui,](#)
955 [K., and Xie, B.: Incorrect Asian aerosols affecting the attribution and projection](#)
956 [of regional climate change in CMIP6 models, *Npj Climate and Atmospheric*](#)
957 [*Science*, 4, \[10.1038/s41612-020-00159-2\]\(https://doi.org/10.1038/s41612-020-00159-2\), 2021.](#)

958 Weart, S.: *The Discovery of Global Warming*, Bibliovault OAI Repository, the
959 University of Chicago Press, 9, [10.2307/3986102](https://doi.org/10.2307/3986102), 2008.

960 Wilcox, L. J., Highwood, E. J., and Dunstone, N. J.: The influence of anthropogenic
961 aerosol on multi-decadal variations of historical global climate, *Environmental*
962 *Research Letters*, 8, [10.1088/1748-9326/8/2/024033](https://doi.org/10.1088/1748-9326/8/2/024033), 2013.

963 Wilcox, L. J., Highwood, E. J., Booth, B. B. B., and Carslaw, K. S.: Quantifying sources
964 of inter-model diversity in the cloud albedo effect, *Geophysical Research Letters*,
965 42, 1568-1575, [10.1002/2015gl063301](https://doi.org/10.1002/2015gl063301), 2015.

966 Williams, K., Copesey, D., Blockley, E., Bodas-Salcedo, A., Calvert, D., Comer, R.,

967 Davis, P., Graham, T., Hewitt, H., Hill, R., Hyder, P., Ineson, S., Johns, T., Keen,
968 B., Lee, R., Megann, A., Milton, S., Rae, J., Roberts, M., and Xavier, P.: The Met
969 Office Global Coupled Model 3.0 and 3.1 (GC3.0 and GC3.1) Configurations, *J.*
970 *Adv. Model. Earth Syst.*, 10, 10.1002/2017MS001115, 2017.

971 Wu, P., Christidis, N., and Stott, P.: Anthropogenic impact on Earth's hydrological
972 cycle, *Nature Climate Change*, 3, 807-810, 10.1038/nclimate1932, 2013.

973 Wu, T., Hu, A., Gao, F., Zhang, J., and Meehl, G.: New insights into natural variability
974 and anthropogenic forcing of global/regional climate evolution, *npj Climate and*
975 *Atmospheric Science*, 2, 10.1038/s41612-019-0075-7, 2019a.

976 Wu, T., Zhang, F., Zhang, J., Jie, W., Zhang, Y., Wu, F., Li, L., Yan, J., Liu, X., Lu,
977 X., Tan, H., Zhang, L., Wang, J., and Hu, A.: Beijing Climate Center Earth System
978 Model version 1 (BCC-ESM1): model description and evaluation of aerosol
979 simulations, *Geosci. Model Dev.*, 13, 977-1005, 10.5194/gmd-13-977-2020, 2020.

980 Wu, T., Lu, Y., Fang, Y., Xin, X., Li, L., Li, W., Jie, W., Zhang, J., Liu, Y., Zhang, L.,
981 Zhang, F., Zhang, Y., Wu, F., Li, J., Chu, M., Wang, Z., Shi, X., Liu, X., Wei, M.,
982 Huang, A., Zhang, Y., and Liu, X.: The Beijing Climate Center Climate System
983 Model (BCC-CSM): the main progress from CMIP5 to CMIP6, *Geosci. Model*
984 *Dev.*, 12, 1573-1600, 10.5194/gmd-12-1573-2019, 2019b.

985 Yool, A., Palmieri, J., Jones, C. G., Sellar, A. A., de Mora, L., Kuhlbrodt, T., Popova,
986 E. E., Mulcahy, J. P., Wiltshire, A., Rumbold, S. T., Stringer, M., Hill, R. S. R.,
987 Tang, Y., Walton, J., Blaker, A., Nurser, A. J. G., Coward, A. C., Hirschi, J.,
988 Woodward, S., Kelley, D. I., Ellis, R., and Rumbold-Jones, S.: Spin-up of UK
989 Earth System Model 1 (UKESM1) for CMIP6, *J. Adv. Model. Earth Syst.*, 12,
990 10.1029/2019ms001933, 2020.

991 Zhang, J., Wu, T., Zhang, F., Furtado, K., Xin, X., Shi, X., Li, J., Chu, M., Zhang, L.,
992 Liu, Q., Yan, J., Wei, M., and Ma, Q.: BCC-ESM1 Model Datasets for the CMIP6
993 Aerosol Chemistry Model Intercomparison Project (AerChemMIP), *Advances in*
994 *Atmospheric Sciences*, 38, 317-328, 10.1007/s00376-020-0151-2, 2021.

995

996

997